Ubiquitin-mediated regulation of RIPK1 kinase activity, independent of IKK and MK2

Alessandro Annibaldi[1,*], Sidonie Wicky John[1,9], Tom Vanden Berghe[2,9], Kirby Swatek[3,9], Jianbin Ruan[4], Hao Wu[4], Gianmaria Liccardi[1], Katiuscia Bianchi[1,5], David Komander[3], Sze Men Choi[2], Samya Van Coillie[2], Peter Vandenabeele[2], John Bertin[6], John Silke[7,8] and Pascal Meier[1,10,*]

1) The Breast Cancer Now Toby Robins Research Centre, Institute of Cancer Research, Mary-Jean Mitchell Green Building, Chester Beatty Laboratories, Fulham Road, London SW3 6JB, UK
2) Inflammation Research Centre, VIB-Ugent, Department of Biomedical Molecular Biology, Ghent, Belgium.
3) Medical Research Council, Laboratory of Molecular Biology, Cambridge, UK
4) Department of Biological Chemistry and Molecular Pharmacology, Harvard Medical School Room 3024B, 3 Blackfan Cir, Boston, MA 02115
5) Centre for Molecular Oncology, Barts Cancer Institute, Queen Mary University of London, London, UK
6) Pattern Recognition Receptor DPU and Platform Technology & Science, GlaxoSmithKline, Collegeville Road, Collegeville, Pennsylvania 19426, United States.
7) The Walter and Eliza Hall Institute of Medical Research, Parkville, Victoria 3052, Australia
8) Department of Medical Biology, University of Melbourne, Parkville, Victoria 3050, Australia
9) These authors contributed equally to this work
10) Lead contact

* Correspondence:
pmeier@icr.ac.uk
Alessandro.Annibaldi@icr.ac.uk
Tel: +44 (0)20 7153 5326
Fax: +44 (0)20 7153 5340

Key words: TNF, cIAPs, Ubiquitin, RIPK1, cell death, caspase-8

Running title: cIAP1-mediated suppression of TNF-induced cell death

SUMMARY

Tumour Necrosis Factor (TNF) can drive inflammation, cell survival and death. While ubiquitylation-, phosphorylation- and NF-κB-dependent checkpoints suppress the cytotoxic potential of TNF, it remains unclear whether ubiquitylation can directly repress TNF-induced death. Here we show that cIAP1 regulates RIPK1 kinase activity not only via activation of downstream kinases and NF-kB transcriptional responses, but also by directly repressing RIPK1 kinase activity via Ubiquitin-dependent inactivation. We find that the UBiquitin-Associated (UBA) domain of cIAP1 is required for optimal Ubiquitin~Lysine occupancy and K48-ubiquitylation of RIPK1. Independent of IKK and MK2, UBA-mediated ubiquitylation suppresses RIPK1 kinase auto-activation and, in addition, marks it for proteasomal degradation. In the absence of a functional UBA domain of cIAP1, more active RIPK1 kinase accumulates in response to TNF, causing RIPK1 kinase-mediated cell death and systemic inflammatory response syndrome. These results reveal a direct role for cIAP-mediated ubiquitylation in controlling RIPK1 kinase activity and preventing TNF-mediated cytotoxicity.

Introduction

Inflammation and cell death are ancient processes of fundamental biological importance that enable survival and adaptation during infection and injury. Tumour necrosis factor (TNF) is a potent inflammatory cytokine that signals, through its type 1 receptor (TNF-R1), either cell survival, cell proliferation or cell death (Quistad and Traylor-Knowles, 2016; Walczak, 2011). TNF stimulates an inflammatory response that removes the sources of disturbance and, ultimately, restores functionality and homeostasis to the tissue. However, when deregulated, inflammation can drive chronic tissue remodelling and repair, which contributes to inflammatory diseases, cancer and treatment failure (Mantovani et al., 2008). Accordingly, TNF plays a pre-eminent role in the development of chronic inflammatory diseases as well as cancer-related inflammation.

In mammals, binding of TNF to its extracellular receptor TNF-R1 triggers either pro-survival/inflammatory or pro-death signalling pathways in a Ub- and phosphorylation-dependent manner (Silke, 2011; Vanlangenakker et al., 2011; Walczak, 2013). TNF can regulate tissue homeostasis in at least three different ways: 1) activation of NF-κB and MAPK/JNK- transcriptional programmes, 2) induction of caspase-8-dependent apoptosis or 3) stimulation of Receptor interacting protein kinase (RIPK)-mediated necroptosis (Declercq et al., 2009).

Binding of TNF to TNF-R1 results in the formation of two signalling complexes (Micheau and Tschopp, 2003). Upon TNF ligation, a protein complex assembles on the cytoplasmic tail of TNFR1. This complex, frequently referred to as complex-I, consists of TNF-R1, the adaptors TRADD, TRAF2, the kinase RIPK1 and the E3 Ubiquitin (Ub)-ligases cellular Inhibitor of APoptosis (cIAP) cIAP1 and cIAP2 (Silke, 2011; Ting and Bertrand, 2016). Within this complex, RIPK1 and other proteins are rapidly conjugated with M1, K11, K48, K63 Ub linkage types (Dondelinger et al., 2016; Dynek et al., 2010; Peltzer et al., 2016). cIAP-mediated conjugation of Ub to RIPK1 allows recruitment of the kinase complex TAK1/TAB2/TAB3 and the E3 ligase Linear Ub chain Assembly Complex (LUBAC, composed of HOIL/HOIP/Sharpin). LUBAC-mediated linear ubiquitylation of different components of

complex-I (RIPK1, TRADD and TNFR1) subsequently reinforces complex-I and allows efficient recruitment and activation of IKK (composed of NEMO/IKKα/IKKβ), which in turn drives activation of NF-κB (Elliott et al., 2016; Hrdinka et al., 2016; Kupka et al., 2016; Schlicher et al., 2016; Silke, 2011; Wagner et al., 2016). While the synthesis of M1- and K63-linked poly-Ub chains play key roles in Ub-dependent assembly of complex-I and the induction of NF-κB target genes that drive inflammation and cell survival following TNF stimulation, the role of K11 and K48 poly-Ub remains largely uncharacterized.

TNF-induced cell death is mediated by a RIPK1-containing secondary complex that is frequently referred to as complex-II or necrosome (Micheau and Tschopp, 2003; Pasparakis and Vandenabeele, 2015; Wang et al., 2008). It is thought that the Ub chains conjugated to RIPK1 by cIAP1/2 and LUBAC in complex-I constitute one of the decisive factors preventing RIPK1 from forming complex-II, and limiting its killing potential (Bertrand et al., 2008; Haas et al., 2009; Peltzer et al., 2016). Consistently, genetic deletion of cIAPs completely abrogates RIPK1 ubiquitylation, leading to exaggerated complex-II formation and RIPK1-mediated cell death in response to TNF (Moulin et al., 2012). The interpretation of the role of RIPK1 ubiquitylation in suppressing the cytotoxic potential of RIPK1 is complicated by the fact that loss of cIAPs not only abrogates RIPK1 ubiquitylation but also interferes with recruitment of LUBAC, TAK1, and IKK. Particularly, loss of TAK1 recruitment prevents activation of MK2 and IKK, which in turn regulate the cytotoxic potential of RIPK1 via direct phosphorylation (Dondelinger et al., 2017; Dondelinger et al., 2015; Jaco et al., 2017; Menon et al., 2017). Thus, loss of cIAPs not only interferes with activation of NF-κB, but also abrogates MK2- and IKK-mediated suppression of RIPK1 (Bettermann et al., 2010; O'Donnell et al., 2007; Vandenabeele and Bertrand, 2012).

While it is beyond doubt that cIAPs suppress TNF-induced cell death, how this is achieved remains unclear. The main problem in dissecting cIAP-mediated regulation of TNF-induced cell death has been the fact that the signaling aspect of Ub (recruitment/activation of TAK1,

IKK, MK2 and NF-κB-mediated gene induction) and the direct Ub-dependent anti-apoptotic function of cIAPs cannot be separated. We now identified a point mutation in cIAP1 that selectively sensitizes cells to TNF-induced cell death, without interfering with TNF-mediated activation of NF-κB, and IKK- and MK2-mediated phosphorylation of RIPK1. This mutation affects the evolutionary conserved UBiquitin-Associated domain (UBA) of cIAP1. Mice with a knock-in mutation in the UBA domain develop normally but are acutely sensitive to TNF-induced systemic inflammatory response syndrome (SIRS), which is caused by enhanced sensitivity to TNF-mediated cell death. Our data are consistent with the notion that the UBA domain is required for Ub-mediated regulation of RIPK1 kinase activity. We find that cIAP1 represses RIPK1 kinase auto-activation via UBA-mediated ubiquitylation of an expanded repertoire of Ub-acceptor lysines of RIPK1. In addition, we find that the UBA domain favours K48-linked poly-ubiquitylation of RIPK1, which, in combination with poly-monoubiquitylation, destabilises active RIPK1 via proteasomal degradation. In the absence of a functional UBA domain, fewer K residues are ubiquitylated, and fewer K48-linked chains are present on RIPK1. Together, this causes lethal accumulation of active RIPK1 kinase in response to TNF in *cIAP1*^{UBAmut} cells. Our data demonstrate, for the first time, that cIAP-mediated ubiquitylation of RIPK1 directly regulates its kinase activity, independently of the recruitment of IKK and TAK1 kinase complexes.

Results

Non-canonical interaction between cIAP1 and TRAF2

The BIR1 and RING domains of cIAP1/2 are required for TNF signalling, but little is known about the role of the UBA domain. Because UBA domains often regulate protein activity via protein-protein interactions (Dikic et al., 2009; Hicke et al., 2005; Yagi et al., 2012), we conducted a yeast two-hybrid experiment with the UBA containing C-terminal portion of cIAP1 (cIAP1$^{U/C/R}$) to establish a UBA interactome of cIAP1 (Figure 1A and 1B). This identified known as well as novel cIAP1 binding proteins (Figure 1B). Surprisingly, out of the 137 clones identified, TRAF2 was isolated 107 independent times. While previous work established that TRAF2 binds to the BIR1 domain of cIAP1 and cIAP2 (Samuel et al., 2006; Vince et al., 2009; Zheng et al., 2010) (Figure 1A), our data suggest that TRAF2 also associates with the C-terminal portion of cIAP1.

To narrow down the region within the UBA-CARD-RING fragment that mediates TRAF2 binding, we trimmed the cIAP1 construct from the C terminus, and determined the ability of these truncated proteins to interact with TRAF2. The UBA domain readily interacted with TRAF2 (Figure 1C and S1A), and point mutations in the conserved MGF motif of the hydrophobic patch of the UBA domain (MF>AA), abrogated the binding of cIAP1 to TRAF2. Consistent with the notion that cIAP1 interacts with TRAF2 through a bimodal interaction via its BIR1 as well as UBA domain, we found that point mutations in either the BIR1 (ER>AA) or UBA domain (MF>AA) did not abolish the interaction between cIAP1 and TRAF2 in yeast-two-hybrid experiments (Figure 1D and 1E, Figure S1B).

To map the region of TRAF2 that bound to the UBA domain we performed further experiments with truncated and mutated TRAF2 variants. Surprisingly, the cIAP-interacting motif (CIM) in the TRAF-N domain, which is required for TRAF2 to interact with the BIR1 of cIAP1 (Vince 2009), was also indispensable for UBA binding. Accordingly, deletion of the 10 amino acid CIM motif completely abrogated the interaction between TRAF2 and the UBA domain of cIAP1 (Figure 1F, S1C). These data indicate that cIAP1 contains two surfaces on very distinct spatially separated domains that somehow bind to the same short TRAF2 motif.

Since TRAF2 forms trimers (Zheng et al., 2010) we cannot discern whether the UBA and BIR1 bind to the very same CIM of one TRAF2 molecule, or to different CIMs of adjacent molecules.

The UBA contributes to TRAF2 binding in solution and in cells

To independently corroborate the interaction, we performed isothermal titration calorimetry (ITC) using recombinant cIAP2. cIAP2 was used instead of cIAP1 because structural information of TFAF2/cIAP2 is known, and all previous ITC measurements involved TRAF2 and cIAP2 (Zheng et al., 2010). Of note, cIAP1's UBA is 87% similar to the one of cIAP2. While the interaction between TRAF2 and the BIR1 domain of cIAP2 exhibits a dissociation constant of 1.7 μM (Zheng et al., 2010), we found that the BIR1 in conjunction with the UBA domain bound to TRAF2 with a significantly higher affinity (0.43 μM) (Figure 2A and 2B). Under the same conditions, the isolated UBA domain bound much less strongly to TRAF2, displaying a dissociation constant of 0.48 mM (Figure 2C).

To determine the importance of the UBA domain for TRAF2 binding in a cellular context, we used *Flp-In*^{TM}*-Rex*^{TM}-HEK293 (hereafter referred to simply as Flp-In) cells. These cells carry a single FRT site, which allows Flp-mediated integration of transgenes into the same transcriptionally regulatable genomic locus. Prior to transgene insertion, isogenic parental HEK293$^{Flp\text{-}In;shcIAP1}$ cells bearing a doxycycline-inducible mir30-based shRNA against the 3'UTR of endogenous *cIAP1* were generated and reconstituted either with WT cIAP1 or the indicated mutants (Figure 2D). Because HEK293$^{Flp\text{-}In}$ cells do not express detectable levels of cIAP2 (data not shown), this system ensures single copy insertion and equal expression levels of untagged cIAP1 proteins without interference from endogenous cIAPs. Expression of the doxycycline-inducible *cIAP1* shRNA in parental cells reduced cIAP1 to an almost undetectable level, and resulted in concomitant activation of the non-canonical NF-κB pathway (Figure 2E). Cells reconstituted with either a WT or a UBA mutant version of cIAP1 exhibited comparable levels of cIAP1, indicating that the UBA mutation did not affect protein stability. Moreover, cIAP1$^{MF>AA}$ suppressed activation of the non-canonical NF-κB pathway (Figure 2E, middle blot, compare lane 2 with lanes 4 and 7), and underwent SM-induced

auto-ubiquitylation and degradation, indicating that cIAP1$^{MF>AA}$ is able to ubiquitylate NIK and itself. Using biotinylated SM as affinity reagent to purify cIAP1 and its binding partners from cellular extracts, we found that it readily co-purified TRAF2 with WT cIAP1 (Figure 2F). In contrast, and consistent with earlier reports (Samuel et al., 2006; Vince et al., 2009; Zheng et al., 2010), we found that mutation of the BIR1 (cIAP1$^{ER>AA}$) almost completely abolished the binding of cIAP1 to TRAF2 (Figure 2F, compare lane 2 with 4). Interestingly, mutation of the UBA domain, either via alteration of the MGF motif (MF>AA) or substitutions of E401 and N428 to RR (EN>RR), which disrupt UBA-mediated protein:protein interactions (Budhidarmo and Day, 2014), likewise impaired TRAF2 binding (Figure 2F and 2G). While mutations in the BIR1 (ER>AA) and the UBA domains (MF>AA) retained some binding to TRAF2, combined mutation in the BIR1 and UBA (ER>AA/MF>AA) completely abrogated the interaction between cIAP1 and TRAF2 (Figure 2F). Together, these data corroborate the notion that TRAF2 interacts with cIAP1 via its BIR1 and UBA domain.

The UBA domain is dispensable for embryonic development and the regulation of canonical as well as non-canonical NF-κB.

To study the importance of the UBA domain of cIAP1 *in vivo*, we generated a conditional knock-in mouse bearing the MF>AA mutation in the absence of cIAP2 (Figure 3A). Previous work indicated that cIAP1 and cIAP2 function redundantly to each other. This is evident as *cIAP1* and *cIAP2* single knock-out (KO) animals are viable and do not exhibit any overt phenotypic abnormalities (Conte et al., 2006; Conze et al., 2005; Moulin et al., 2012), whereas *cIAP1*/*cIAP2* double knock-out (DKO) animals die at embryonic stage E10.5 due to cardiovascular defects (Moulin et al., 2012). Due to the redundant nature of these cIAPs, we generated the conditional *cIAP1*^{UBAmut} mouse from an ES cell clone that previously had been targeted at the *cIAP2* locus (Moulin et al., 2012). These doubly targetted animals (*cIAP2*$^{-/-}$ *cIAP1*^{UBAmut}) are subsequently referred to as *cIAP1*^{UBAmut}. *cIAP1*^{UBAmut} mice were born and weaned at the expected Mendelian ratio (Figure 3B), and were indistinguishable from their *WT* counterparts (Figure S2A and S2B). Additionally, these mice had an overtly normal immune system, with T and B cells as well as cells of myeloid origin equally represented in *WT* and *cIAP1*^{UBAmut} mice (Figure S2C). Primary mouse embryonic fibroblasts (MEFs)

isolated from WT and *cIAP1*^{UBAmut} E13.5 embryos exhibited the same cIAP1 protein levels (Figure 3C), indicating that the UBA mutation had no impact on the stability of cIAP1. As expected, these cells exhibited undetectable levels of *cIAP2* mRNA (Figure S2D). To verify whether the UBA mutation affected cIAP1's E3 ligase function, we tested the ability of SM to stimulate auto-ubiquitylation and degradation of cIAP1^{UBAmut}. We found that the behaviour of cIAP1^{UBAmut} was indistinguishable from its wild-type counterpart (Figure S2E).

To confirm the importance of the UBA domain for the binding to TRAF2, we purified cIAP1 using biotinylated SM in *cIAP2*$^{-/-}$, *cIAP1*^{UBAmut}, and *Traf2*$^{-/-}$ mouse embryonic fibroblasts. *cIAP2*$^{-/-}$ cells were chosen as control given the absence of *cIAP2* in the *cIAP1*^{UBAmut} cells. We found that significantly less TRAF2 was co-purified with cIAP1 in *cIAP1*^{UBAmut} cells, while no TRAF2 binding was observed in *TRAF2*$^{-/-}$ cells (Figure 3D), confirming the data obtained with reconstituted human cells (Figure 2F-G). Importantly however, while this immunoprecipitation setting reveals a weakened association between cIAP1^{UBAmut} and TRAF2, under physiological conditions cIAP1 and TRAF2 are perfectly capable of interacting with each another. This is evidenced because the UBA mutation of cIAP1 does not phenocopy loss of TRAF2 (Figure 3E). Accordingly, RIPK1 is readily poly-ubiquitylated in complex-I in cells from *cIAP1*^{UBAmut} animals, while RIPK1 ubiquitylation is lost in *Traf2 KO* cells (Figure 3E). Moreover, cIAP1:TRAF2-mediated regulation of NIK, and suppression of non-canonical NF-κB, is normal in *cIAP1*^{UBAmut} animals (Figure 3F). On the other hand, depletion of cIAP1^{WT} and cIAP1^{UBAmut} by SM or depletion of TRAF2 by TWEAK (Vince et al., 2008) activates non-canonical NF-κB (Figure 3F). As TRAF2 is essential to bring cIAPs to NIK, this data demonstrate that cIAP1^{UBAmut}:TRAF2 association is sufficiently strong *in vivo* to target NIK for ubiquitylation and degradation. Additionally, the UBA domain of cIAP1 was entirely dispensable for timely TNF-induced phosphorylation and activation of p65, degradation of IκB, phosphorylation of MAPKs (Figure 3G and S2F), and the production of cytokines in primary MEFs (Figure 3H and 3I), BMDMs (Figure 3J) and keratinocytes (Figure 3K). Taken together, our data demonstrate that cIAP1^{UBAmut} retains E3 ligase activity, and that the UBA domain is dispensable for embryonic development or routine tissue homeostasis. Additionally, we conclude that the UBA domain of cIAP1 is not required for RIPK1 ubiquitylation in

complex-I, suppression of the non-canonical and activation of the canonical NF-κB pathway.

UBA mutant mice develop normally but are acutely sensitive to TNF-induced systemic inflammatory response syndrome (SIRS)

Next we determined the response of *cIAP1*^{UBAmut} mice to TNF challenge. Injection of TNF provokes systemic inflammation that is driven by RIP kinase-dependent cell death (Duprez et al., 2011) and resembles clinical systemic response syndrome (SIRS) (Tracey et al., 1986). Strikingly, *cIAP1*^{UBAmut} mice were much more sensitive to TNF-induced SIRS than wild-type and *cIAP2*$^{-/-}$ counterparts. Accordingly, following administration of a dose of murine TNF as low as 4 μg/Kg of body weight, *cIAP1*^{UBAmut} mice exhibited a dramatic drop in body temperature and significant increase in morbidity (Figure 4A and 4B). TNF treated *cIAP1*^{UBAmut} mice also had significantly elevated levels of aspartate transaminase (AST), alanine transaminase (ALT) and lactate dehydrogenase (LDH) in the plasma indicating liver and tissue damage (Figure 4C and 4D). Consistently, livers from *cIAP1*^{UBAmut} mice had considerably higher numbers of TUNEL positive cells than *cIAP2*$^{-/-}$ or *WT* littermate control mice, (Figure 4E and 4F). Collectively, these data demonstrate that the UBA of cIAP1 is required to protect mice from the lethal effects of TNF.

Mutation in the UBA domain switches the TNF response to cell death

To examine the role of the UBA domain in regulating the cellular response to TNF we used primary bone marrow-derived macrophages (BMDMs), mouse dermal fibroblasts (MDFs) and embryonic fibroblasts (MEFs). TNF treatment did not induce substantial cell death in either wild-type or cIAP2 deficient cells, however it was a potent cell death stimulus in *cIAP1*^{UBAmut} cells (Figure 5A, 5C, 5D, S3A and S3B). This cell death was RIPK1 kinase dependent because treatment with the selective RIPK1 inhibitor GSK'963 (Berger et al., 2015) suppressed TNF killing. Likewise, primary *cIAP1*^{UBAmut} BMDMs were exquisitely more sensitive to RIPK1-mediated TNF-induced necroptosis than BMDMs from either wild-type littermates or single targeted *cIAP2*$^{-/-}$ animals (Figure 4A). Consistently, increased association of RIPK1 with RIPK3 was detected by Proximity Ligation Assay (PLA) (Figure 5B). Primary MDFs and MEFs instead seemed to die by apoptosis since RNAi-mediated depletion of MLKL

had no apparent effect on TNF-induced cell death in *cIAP1*^{UBAmut} MEFs (Figure S3D). Consistently, TNF stimulation of *cIAP1*^{UBAmut} MDFs and MEFs caused elevated levels of caspase activity (Figure S3E), which was accompanied with enhanced complex-II formation (Figure 5D and 5F), and cleavage and activation of caspase-8 and caspase-3 (Figure S3F). Importantly, *cIAP1*^{UBAmut} MEFs prepared from multiple embryos within the same litter and between litters behaved in the same manner (Figure S3A, S3B and S3C). Together, these data suggest that the UBA domain allows cIAP1 to inhibit TNF induced death.

The UBA directly regulates RIPK1 ubiquitylation

Since ubiquitylation of RIPK1, and other components of complex-I, represses RIPK1-dependent formation of complex-II, we analysed complex-I formation in MDFs and MEFs. As previously reported, deficiency of cIAP1 and cIAP2 prevented ubiquitylation of RIPK1 and the recruitment of the LUBAC components SHARPIN and HOIL five minutes after TNF stimulation (Figure 6A, compare lane 2 to 5) (Haas et al., 2009). We found no evidence for defective ubiquitylation of RIPK1 in complex-I in single targeted *cIAP2*$^{-/-}$, but cIAP1 deficient MEFs had significantly lower molecular weight modified forms of RIPK1, and substantial levels of non-modified RIPK1. *cIAP1*^{UBAmut} cells, however, displayed a more marked and reproducible decrease in the extent of high molecular weight RIPK1 ubiquitylation (arrows) in complex-I in both MEFs and MDFs (Figure 6A, 6B and S4A), compared to *cIAP2*$^{-/-}$ and WT cells. Importantly, the extent of non-modified RIPK1 in complex-I was indistinguishable between *WT*, *cIAP2*$^{-/-}$ and *cIAP1*^{UBAmut} cells (Figure 6A and 6B, see quantifications), suggesting that the same amount of RIPK1 undergoes ubiquitin modifications in these three genotypes. Because the same amount of RIPK1 is being ubiquitylated in *WT*, *cIAP2*$^{-/-}$ and *cIAP1*^{UBAmut} cells, but overall ubiquitylation of RIPK1 seems to be affected in *cIAP1*^{UBAmut} cells compared to *WT* and *cIAP2*$^{-/-}$ cells, we conclude that RIPK1 undergoes Ub modifications that are distinct from those observed in wild-type, *cIAP1*$^{-/-}$ *or cIAP2*$^{-/-}$ cells. Although the UBA mutation resulted in reduced levels of ubiquitylated RIPK1 in complex-I, this had no apparent effect on the kinetics of the recruitment of other components of the TNF-RSC such as SHARPIN and HOIL-1 (Figure 5A and 5B).

Next, we addressed whether the weakened association of cIAP1^{UBAmut} with TRAF2 might lead to decreased recruitment of cIAP1 to complex-I and generally decreased ubiquitylation mediated by cIAP1 (Figure 6A, compare lane 11 to 14 and 6B, compare lane 8 to 11 for cIAP1 levels). To this end, we increased the amount of cIAP1^{UBAmut} to the levels of WT cIAP1 in complex-I using a Doxocycline-inducible reconstitution approach. This allowed us to induce the expression of cIAP1^{UBAmut} so that comparable amount of cIAP1^{UBAmut} protein was present in complex-I as in *WT* or *cIAP2* KO cells (Figure 6C, compare lane 2 to 5). Even though the levels of cIAP1^{UBAmut} in complex-I was comparable to cIAP1-WT, this did not 'normalise/correct' the ubiquitylation pattern of RIPK1, nor did it have an impact on the recruitment of unmodified RIPK1 in complex-I (Figure 6C, compare lane 5 to 8). This demonstrates that the different smearing pattern of ubiquitylated RIPK1 in the *cIAP1*^{UBAmut} cells is not due to impaired recruitment of cIAP1 to complex-I, and, therefore, are not TRAF2-binding-dependent but merely UBA dependent.

The UBA is required for efficient K48-ubiquitylation and degradation of RIPK1 in complex-I

To provide a robust analysis of the composition of Ub linkage types on RIPK1 in *cIAP2*$^{-/-}$ and *cIAP1*^{UBAmut} cells, we employed absolute quantification (AQUA)-based mass spectrometry of RIPK1 in complex-I. To this end, we performed two consecutive immunoprecipitiations (IP), first of complex-I (FLAG-TNF) and then of RIPK1 (Figure 7A). Following double purification, retained ubiquitylated RIPK1 was subject to tryptic digestion, and the eluate was spiked with isotope-labelled GlyGly-modified AQUA peptide standards derived from each linkage type, allowing AQUA-based absolute quantification of all chain types. Our analysis revealed that K48-linked chains on RIPK1 were reproducibly less abundant (13% reduction) in *cIAP1*$^{UBAmut,cIAP2-/-}$ mutant cells compared to *cIAP2*$^{-/-}$ (Figure 7A). Beside K63-linked Ub chains, no other linkage types were reproducibly detected on RIPK1. Calculations from the AQUA-based mass spectrometry experiment indicated that the majority of Ub is conjugated in the form of mono-Ub moieties (data not shown) rather than chains, and that the actual chains on RIPK1 are surprisingly short, even in the control situation. Given that the overall smearing pattern is reduced in *cIAP1*^{UBAmut} cells, this suggests that not only K48-ubiquitylation is

affected but also that the occupancy of acceptor lysine (K) residues is altered.

To test the possibility that the occupancy of acceptor K of RIPK1 from *cIAP1*^{UBAmut} cells differs from the one in control *cIAP2*$^{-/-}$ cells, we analysed ubiquitylated RIPK1 from complex-I using Ub chain restriction (UbiCRest) (Hospenthal et al., 2015) (Figure 7B). To this end, we used a combination of deubiquitylating enzymes (vOTU/OTULIN) that remove all chain types but leave the most proximal Ub attached to RIPK1. vOTU hydrolyses all Ub-linkage types except M1-linked chains, which can be cleaved by OTULIN. Incubation with vOTU/OTULIN revealed a reduction in the Ub-site occupancy in *cIAP1*^{UBAmut} compared to *cIAP2*$^{-/-}$ (Figure 7B, compare lane 5 with 10). The reduced Ub occupancy of RIPK1 might help to explain the shift towards the lower molecular weights of ubiquitylated RIPK1 in *cIAP1*^{UBAmut} cells.

Since K48-linked chains as well as poly-mono-ubiquitylation can target proteins for degradation (Braten et al., 2016), we tested whether the combined reduction in poly- and mono-ubiquitylation of RIPK1 affects the protein stability of RIPK1 in complex-I. Using Tandem Ub Binding Entities (TUBE) (Hjerpe et al., 2009), which allow isolation of polyubiquitylated proteins, we found that the levels of ubiquitylated RIPK1 dramatically accumulated in *cIAP1*^{UBAmut} cells compared to *WT* cells over a 6 hours time period following TNF treatment (Figure 7C). Importantly, TNF-induced accumulation of ubiquitylated RIPK1 in *cIAP1*^{UBAmut} cells coincided with a significant increase in formation of complex-II and activation of caspase-8 (Figure 7C, bottom three panels). This demonstrates that the UBA domain of cIAP1 represses lethal accumulation of RIPK1, most likely by facilitating efficient poly-mono as well as K48-mediated ubiquitylation and degradation of RIPK1, which would lower the number of 'seeding' molecules for formation of complex-II (Jaco et al., 2017). Importantly, while ubiquitylated RIPK1 accumulated over time in TNF-treated *cIAP1*^{UBAmut} cells, treatment of *cIAP1*^{UBAmut} cells with proteasome inhibitors (MG132) did not result in a further increase in RIPK1 accumulation (Figure 7D), corroborating the notion that the stabilization effect is due to the UBA mutation. While treatment with MG132 did not cause a further stabilization of RIPK1 in *cIAP1*^{UBAmut} cells, proteasome inhibition in *WT* cells resulted in a substantial accumulation of RIPK1 in the ubiquitylated proteome (Figure S5A), indicating that under normal conditions

RIPK1's stability is regulated, at least in part, in a Ub- and proteasome-dependent fashion. Of note, since RIPK1 forms amyloid like structures upon activation, the TUBE-based experiment also purifies non-ubiquitylated RIPK1 that is bound to ubiquitylated RIPK1. We also addressed whether the UBA domain might shield ubiquitylated RIPK1 from DUBs. However, using a broad-spectrum DUB inhibitor (PR619), we found no evidence for a role of the UBA domain in protecting ubiquitylated RIPK1 from DUB digestion (Figure S5B and S5C).

UBA-mediated ubiquitylation of RIPK1 represses its kinase activity

RIPK1 functions as a scaffold molecule for TNF-mediated gene activation, and as a kinase to drive apoptosis or necroptosis (Berger et al., 2014; Peltzer et al., 2016). TNF-induced activation of IKK and MK2 directly suppresses the kinase activity and cytotoxic potential of RIPK1 (Dondelinger et al., 2017; Dondelinger et al., 2015; Jaco et al., 2017; Menon et al., 2017). In particular, MK2 directly phosphorylates mouse RIPK1 at serine (S) 321 and S336 (S320 and S335 in human), which in turn suppresses RIPK1 auto-activation at S166 (Dondelinger et al., 2017; Jaco et al., 2017; Menon et al., 2017). Since *cIAP1*^{UBAmut} cells are sensitised to RIPK1 kinase mediated cell death in response to TNF, we addressed whether the UBA mutation affects MK2-mediated suppression of RIPK1 kinase activity. RIPK1 immuno-precipitation from TNF-treated *cIAP2*$^{-/-}$ and *cIAP1*^{UBAmut} cells revealed a strong increase in auto-phosphorylation at S166 in *cIAP1*^{UBAmut} cells, which is entirely consistent with the notion that TNF causes auto-activation of RIPK1, and RIPK1 kinase-dependent cell death in these cells (Figure 7E). Intriguingly, activation of MK2 and MK2-mediated phosphorylation of S321 was entirely normal in *cIAP1*^{UBAmut} cells, demonstrating that activation of RIPK1 kinase activity in *cIAP1*^{UBAmut} cells was MK2-independent. Similarly, timely activation of IKK and NF-κB-mediated expression of target genes was as in *WT* and *cIAP2*$^{-/-}$ cells (Figure 3G to 3J), suggesting that IKK-mediated regulation of RIPK1 is unlikely to be perturbed in *cIAP1*^{UBAmut} cells. In agreement with this view we found that inhibition of IKK with TPCA-1 further sensitised *cIAP1*^{UBAmut} cells to TNF killing (Figure 7F).

Together, out data are consistent with a model whereby cIAP1 regulates RIPK1 kinase activity not only by activating downstream kinases, such as IKK and MK2, but also by directly repressing RIPK1 kinase activity via Ub-dependent inactivation. The conjugation of Ub to RIPK1 might impede its auto-activation and, in addition, mark it for proteasomal degradation, thereby limiting accumulation of cytotoxic RIPK1.

Discussion

Although it is clear that TNF signals cell survival and death, the molecular mechanisms that can switch between the distinct outcomes remain ill defined. Ub-mediated inactivation of RIPK1 has long been postulated to contribute to the regulation of cytokine-induced cell death (Ea et al., 2006; Moquin et al., 2013; O'Donnell et al., 2007). However, detailed insights into the determinants and the actual molecular and functional consequences of RIPK1 ubiquitylation have not been demonstrated. Here we show that the UBA domain of cIAP1 interacts with TRAF2 and is required for proper regulation of RIPK1 kinase activity. In the absence of a functional UBA domain, more active RIPK1 kinase accumulates in response to TNF, causing RIPK1 kinase-mediated cell death and systemic inflammatory response syndrome.

UBA-mediated ubiquitylation of RIPK1 seems to regulate RIPK1 kinase activity through two potentially interconnected mechanisms: First, the UBA domain is required for optimal Ub occupancy of RIPK1. This is evident as fewer K residues are conjugated to Ub in cells from *cIAP1*^{UBAmut} animals. While this reduction in ubiquitylation of RIPK1 has no effect on its scaffolding function, such as activation of TAK1, IKK, MK2, the induction of NF-κB target genes and the production of cytokines, reduced RIPK1 ubiquitylation severely compromises proper regulation of RIPK1 kinase activity, leading to enhanced RIPK1 auto-phosphorylation and formation of complex-II. Second, the UBA domain of cIAP1 also contributes to the regulation of cytotoxic potential of RIPK1 by targeting it for proteasomal degradation. In the absence of a functional UBA domain, fewer poly-mono and K48-linked chains are conjugated to RIPK1 in complex-I.

Although the overall difference in K48-ubiquitylation of RIPK1 is a mere 13%, this causes a significant alteration of RIPK1's stability as active, ubiquitylated RIPK1 accumulates over time in *cIAP1*^{UBAmut} cells. Since K48-linked chains as well as poly-mono-ubiquitylation can target proteins for degradation (Braten et al., 2016) it is highly likely that the combined reduction in poly- and mono-ubiquitylation of RIPK1 ultimately contributes to the increased protein stability of RIPK1 in complex-I from *cIAP1*^{UBAmut} cells, leading to exacerbated RIPK1 kinase activity in

response to TNF. Thus, under normal conditions, the conjugation of Ub to RIPK1 might impede its auto-activation and, in addition, mark it for proteasomal degradation, thereby limiting accumulation of cytotoxic RIPK1. Clearly, the ability of cIAP1 to suppress the cytotoxic potential of RIPK1 not only depends on UBA-mediated regulation of RIPK1. In addition to the above-mentioned regulation, cIAP1 represses RIPK1 auto-activation by facilitating Ub-mediated recruitment of LUBAC and activation of IKK and MK2. While it is currently unclear how LUBAC supresses RIPK1 kinase activity, Ub-mediated recruitment and/or activation of IKK and MK2 reportedly regulate RIPK1 kinase activity through inhibitory phosphorylation (Dondelinger et al., 2017; Dondelinger et al., 2015; Jaco et al., 2017; Menon et al., 2017). Our current data are consistent with a revised model for TNF signalling whereby RIPK1's kinase activity is suppressed through both Ub-mediated phosphorylation of RIPK1 by IKK and MK2 as well as by direct Ub-mediated inactivation and degradation of RIPK1. Therefore, kinase- and Ub-mediated regulation of RIPK1 serve as survival checkpoints for cell fate in inflammation.

The ability of cIAP1 to target RIPK1 for degradation depends on activation of TNFR1. In the absence of receptor engagement, cIAP1 does not regulate RIPK1 levels, potentially because HSP90 sequesters RIPK1 in its monomeric, kinase inactive state (Lewis et al., 2000). Thus, under resting conditions, RIPK1 seems to reside in an inactive configuration that precludes cIAP1/TRAF2 binding. Only when it is recruited to TNFR1 does it get into proximity of cIAP1/TRAF2. In this respect, cIAP1 may sense the activity status of RIPK1. Recruitment of cIAP1 to TNF-RSC reportedly depends on TRAF2. Unexpectedly, we find that the UBA domain of cIAP1 contributes to efficient TRAF2 binding. Consistent with the notion that cIAP1 interacts with TRAF2 through a bimodal interaction via its BIR1 as well as UBA domain, we find that point mutations in either the BIR1 or UBA domain weakens the interaction between cIAP1 and TRAF2. Although cIAP1^{UBAmutant} proteins bind less well to TRAF2 in co-immunoprecipitation studies under resting conditions, under *in vivo* settings this association is sufficient to maintain TNF-induced activation of NF-κB or support TRAF2/TRAF3-mediated degradation of NIK. Importantly, despite the fact that UBA mutant cIAP1 interacts less efficiently with TRAF2 under IP conditions, the reduced ubiquitylation of RIPK1 in complex-I

observed in *cIAP1*^{UBAmutant} cells is not due to impaired cIAP1 recruitment. This is evident as elevating the levels of cIAP1^{UBAmut} expression, which causes a corresponding increase in cIAP1^{UBAmut} recruitment into complex-I that is comparable to the one of *WT* or *cIAP2*$^{-/-}$ cells, does not 'normalise/correct' the ubiquitylation pattern of RIPK1. Further evidence is provided by the fact that the UBA mutation of cIAP1 does not phenocopy loss of TRAF2. Accordingly, RIPK1 is readily ubiquitylated in complex-I in cells from *cIAP1*^{UBAmut} animals. In contrast, RIPK1 ubiquitylation in complex-I is completely lost in TRAF2 KO cells. Taken together, our data demonstrate that cIAP1^{UBAmut} retains E3 ligase activity, and that the UBA domain is dispensable for embryonic development or routine tissue homeostasis. Additionally, we conclude that the UBA domain of cIAP1 is not required for (i) K63-ubiquitylation of RIPK1 in complex-I, (ii) suppression of the non-canonical and (iii) activation of the canonical NF-κB pathway. Consistently, cells lacking a functional UBA do not show any deficit in TNF-induced activation of NF-κB, MAPK signalling or the production of pro-inflammatory cytokines. Thus, the elevated sensitivity to the cytotoxic potential of TNF cannot be explained by the regulation of NF-κB or MK2. We propose that the UBA mutation provides rare insight into the protein architecture of complex-I. We suggest that the UBA contributes to the proper positioning of the RING domain of cIAP1 within complex-I so that the Ub-loaded E2 enzyme can optimally transfer ubiquitin to RIPK1.

As TNF is a key player in the cytokine network that supports inflammation-associated cancer, and cancer-related inflammation (Mantovani et al., 2008) it will be important to gain a better understanding of the checkpoints that control life and death decisions in response to TNF. A better understanding of such checkpoints could lead to new approaches for the treatment of chronic inflammatory diseases that are fueled by aberrant RIPK1-induced cell death, and/or reveal novel strategies for anti-cancer immunotherapies that harness RIPK1's ability to trigger immunogenic cell death (Yatim et al., 2015).

METHODS

Mice generation

The cIAP2 and cIAP1 genes are positioned 10 Kb apart on the same chromosome. Hence, they recombine as a single genomic locus. The *cIAP2*$^{FRT/FRT}$*cIAP1*^{minigene} mouse was generated by electroporating the *cIAP1* targeting vector into *C57BL6*-derived ES cells that were previously targeted on the *cIAP2* locus (Moulin et al., 2012). For the cIAP1 targeted allele the M396A and F398A mutations were introduced into exon 4 and a *F3* site-flanked *PGK-Hygro* selection cassette was inserted upstream of the genetically altered exon 4. A mini-gene corresponding to exon 4-7 of cIAP1 and a BGH poly-A signal were placed upstream of the selection cassette. The cDNA mini-gene is flanked by *loxP* sites. Mice carrying the *cIAP2*$^{FRT/FRT}$*cIAP1*^{minigene} alleles were crossed to transgenic mice expressing the *FLPo* recombinase to generate the *cIAP2*$^{-/-}$*cIAP1*^{minigene} animals. The *PGK-Hygro* resistance cassette on the cIAP1 targeted allele was also deleted by the FLPo-mediated recombination. The *cIAP2*$^{-/-}$*cIAP1*^{minigene} mice were subsequently crossed to transgenic mice expressing the *Cre* recombinase to delete the mini-gene and generate the *cIAP2*$^{-/-}$*cIAP1*^{UBAmut} animals. *cIAP2*$^{-/-}$*cIAP1*$^{loxP/loxP}$ mice were a gift from John Silke, and were previously described (Moulin et al., 2012).

Mice injections monitoring and sampling

Experiments in mice were performed at the Department of Pharmacology of the Faculty of Veterinary Medicine of the Ghent University, Belgium, according to institutional, national and European regulations. Animal protocols were approved by the ethics committee of Ghent University. mTNF was diluted in endotoxin-free PBS and injected intravenously (i.v.) in a volume of 0.2 ml. Rectal body temperature was recorded with a digital thermometer (model 2001; Comark Electronics). Plasma samples and tissue samples of liver were collected at designated times after injection. Blood was obtained by cardiac puncture.

Isolation of primary cells

Primary Mouse Embryonic Fibroblasts (MEFs) were generated from E13.5 embryos. After removing the placenta, yolk sac, head and the dark red organs, embryos were finely minced and digested for 20 min in 0.25 % trypsin. Single cell suspension was then obtained by pipetting up and down the digested embryos. Mouse Dermal Fibroblasts (MDFs) were isolated as described in (Etemadi et al., 2015). To generate Bone Marrow Derived Macrophages (BMDMs), bone marrow cells from tibia and femur of 2 month old mice were seeded in non-coated petri dishes and cultured for 6 days in Dulbecco's modified Eagle medium + 10 % fetal bovine serum + 20 % (v/v) L929 mouse fibroblast conditioned medium. Keratinocytes were isolated as described in (Lichti et al., 2008). Splenocytes were isolated from 2 month old mice. Mouse spleens were mashed through a cell strainer into the petri dish using the plunger end of a syringe. Cells were then washed once in cold PBS and treated

with 1X Red Blood Cell Lysis Buffer (BioLegend, Cat N 420301) for 5 min on ice. Cells were then washed again in PBS and counted.

Splenocytes FACS analysis

5 x 10^5 splenocytes were resuspended in 500 µl of cold PBS and stained with DAPI (1/5000) for 20 min on ice. Cells were then washed with cold PBS and resuspended in 50 µl Staining Buffer. 2 µl of blocking antibody (Anti-Mouse CD16/CD32) were added, and cells were kept on ice for 10 min. 50 µl of Staining Buffer containing the desired antibodies were then added and cells were kept on ice for 30 min. Cells were washed in cold PBS, resuspended in 1 ml of cold PBS and analysed by FACS.

Cell culture, constructs and transfection

Primary MEFs, MDFs and *Flp-In^{TM}-Rex^{TM}-HEK293* cells were cultured in Dulbecco's modified Eagle's Medium (DMEM) supplemented with 10 % Fetal Bovine Serum (FBS), penicillin and streptomycin under 10 % CO2. For the generation of the 293 stable cell lines, where endogenous cIAP1 was reconstituted with WT and mutant cIAP1, *Flp-InTM T-RExTM HEK293^{shcIAP1}* cells were created. First *Flp-In^{TM}T-REx^{TM}-HEK293* cells (Invitrogen) were transduced with lentiviral particles targeting the 3' UTR of the *cIAP1* mRNA. To this end, we used *pTRIPZ-shcIAP1* (Open Biosystems), which allows Doxocycline-inducible expression of a miR30-based *shcIAP1* RNA. After puromycin selection, individual clones were tested for *cIAP1* knockdown efficiency. Such cells were further tested functionally using TNF signalling and NIK activation as readouts. Next, the respective *cIAP1* constructs were cloned into *pcDNA5.1/FRT/TO* (Invitrogen). The empty *pcDNA5.1/FRT/TO-2HA-Strep* plasmid was used as a control. To generate site-specific single copy insertions, *pcDNA5.1FRT/TO*-based plasmids were co-transfected with *pOG44* into *Flp-In^{TM}T-REx^{TM}-HEK293^{shcIAP1}* cells. After selection with hygromycin, stable cells were selected. Endogenous cIAP1 suppression and expression of WT or mutant versions of cIAP1 were simultaneously induced by treating cells with 100 ng/ml Doxycycline for at least 48 hours.

Reagents, Constructs and Antibodies

The GSK'963 RIPK1 kinase inhibitor was provided by GSK. The following antibodies were used: α-RIPK1 (BD Biosciences, 610459), α-HOIL (gift from Henning Walczak), α-cIAP1 (Enzo, ALX-803-335-C100), α-TNFR1 (Abcam, 19139), α-Actin (Santa Cruz Biotechnology, sc-1615), α-P-p65 (Cell Signaling, 3033), α-p65 (Cell Signaling, 8242), α-IkBα (Santa Cruz, sc-371), α-P-p38 (Cell Signaling, 9215), α-p38 (Cell Signaling, 9212), α-P-JNK (Cell Signaling, 9255), α-JNK (Santa Cruz Biotechnology, sc-571), α-P-ERK (Cell Signaling, 9101), α-ERK (gift from Chris Marshall) α-caspase-8 (Cell Signaling, 9429), α-FLAG [M2] (SIGMA, M8823), α-Ub (Dako, Z0458), α-FLIP (Adipogene, AG-20B-0056), α-FADD (Santa Cruz Biotechnology, sc-6036), α-RIPK3 (ProSci, 2283), α-Tubulin (SIGMA, T9026), α-SHARPIN (Proteintech, 14626-1-AP), α-TRAF2 (Cell Signaling, 4712), α-CD8-PE-Cy7, GR-1-PE-Cy7,

CD11c-FITC, CD4-FITC, CD11b-Cy5, B220-FITC (gift from Henning Walczak), α-CD69-PE (eBioscience, 12-0691-82), α-CD3-APC (eBioscience, 47-0032-82), and α-CD16 (eBioscience, 14-0161-82).

UbiCRest analysis

The UbiCRest analysis with linkage selective DUBs was performed essentially as described in (Hospenthal et al., 2015). Briefly, the release fraction (see complex-I purification) was incubated with the following DUBs: 1 µM OTULIN, 0.5 µM vOTU, 1.5 µM USP21. The reaction was conducted in the presence of 1 mM DTT for 30 min at 37 °C. Reactions were stopped with SDS sample buffer, and the ubiquitylation status analysed by western blotting.

Tube Assay

Cells were lysed in DISC lysis buffer (20 mM Tris-HCL pH7.5, 150 mM NaCl, 2 mM EDTA, 1 % Triton X-100, 10 % glycerol) supplemented with protease inhibitors, 1 mM DTT, PR619 (10 µM) and GST-TUBE (50 µg/ml; 50 µg TUBE/mg protein lysate). Cell lysates were rotated at 4°C for 20 min then clarified at 4 °C at 14,000 rpm for 10 min. 20 µl GST beads were added and immunoprecipitations were performed overnight. Beads were washed 4x in wash buffer (50 mM Tris pH 7.5, 150 mM NaCl, 0.1 % Triton X-100, and 5 % glycerol) + PR619 (10 µM), and bound proteins eluted by boiling in 50 µ l 1x SDS loading dye.

Complex-I/II Purification

Cells were seeded in 15 cm dishes and treated as indicated with 3x FLAG-hTNF (5 µg/ml). To terminate stimulation, media was removed and plates were washed with 50 ml of ice cold PBS. Plates were frozen at -80 °C until all time points were acquired. Plates were thawed on ice and cells were lysed in 1 % Triton X-100 lysis buffer (30 mM Tris-HCl pH 7.4, 120 mM NaCl, 2 mM EDTA, 2 mM KCl, 10% glycerol and 1 % Triton X-100, supplemented with protease inhibitors and PR619 (10 µM). Cell lysates were rotated at 4 °C for 20 mins then clarified at 4 °C at 14,000 rpm for 30 mins. Proteins were immunoprecipitated from cleared protein lysates with 20 µl of α-FLAG M2 beads (SIGMA) with rotation overnight at 4°C. For the 0 hr sample 5 µg/ml of FLAG-TNF were added post-lysis. 4x washes in 1 % Triton X-100 buffer with PR619 (10 µM) were performed, and samples eluted by boiling in 60 µl 1x SDS loading dye. For complex-II purification cells were seeded in 10 cm dishes and treated as indicated using media containing 1x FLAG-TNF (100 ng/ml) and zVAD (10 µM). Cells were lysed on ice in 1 % Triton X-100 lysis buffer (30 mM Tris-HCL pH 7.4, 120 mM NaCl, 2 mM EDTA, 2 mM KCl, 1 % Triton X-100 supplemented with protease inhibitors and 10 µM PR619). Cell lysates were rotated at 4 °C for 20 mins then clarified at 4 °C at 14,000 rpm for 10 mins. 20 µl of protein G sepharose (SIGMA), blocked for 1 hr with lysis buffer containing 1 % BSA, were bound with FADD antibody (1.5 µg antibody/mg protein lysate) and were rotated with cleared protein lysates 4 hrs at 4 °C. 4x washes in lysis buffer were performed, and samples eluted by boiling in 80 µl 1x SDS sample buffer.

Cell death analysis

2 x 10^5 cells (MEFs and MDFs) were seeded in six well plates and 24 hrs later they were treated as indicated for an additional 24 hrs. Hoechst 33342 (10 µg/ml) and Propidium Iodide (PI) (1 µg/ml) were added. After 2 mins 10 to 15 images per well were taken with a fluorescent inverted microscope and the ration of dead/live cells were counted manually. 5 x 10^4 BMDMs were seeded in 96 well plates and 24 hrs later they were treated as indicated for an additional 24 hrs. Hoechst (0.5 µg/ml) and PI (1 µg/ml) were added and the ratio dead/live cells was measured using the Celigo imaging system.

Production of recombinant proteins and isothermal titration calorimetry

Various human *cIAP2* and *TRAF2* segments were cloned into *pSUMO* vector respectively to produce N-terminally His-SUMO tagged proteins. The constructs were then transformed into BL21 (DE3) cells and cultured in LB medium at 37 ^{o}C, respectively. Protein expression was induced overnight at 20 ^{o}C with 0.5 mM IPTG when OD_{600} reached 0.8. Cells were lysed in buffer containing 25 mM Tris-HCl at pH 8.0, 150 mM NaCl, 10 mM imidazole and 5 mM β-mercaptoethanol. The recombinant proteins were affinity-purified by Ni-Sepharose beads (GE Healthcare Life Sciences). The SUMO tag was removed by overnight digestion with homemade ULP1 protease at 4 °C. The untagged proteins were further purified by HiTrap Q anion exchange and Superdex 200 gel filtration chromatography (GE Healthcare Life Sciences). Isothermal titration calorimetry measurements were performed at 16 °C, using a MicroCal ITC_{200} microcalorimeter (MicroCal Inc.). For the TRAF2:cIAP2 interactions, the calorimetric titrations were performed by injecting 2 µl of cIAP2 protein solution (2–4 mM) into a sample cell containing 200 µl 0.20 mM TRAF2 protein in 25 mM Tris-HCl at pH 8.0, 150 mM NaCl. A total of 20 injections were performed with a spacing of 150 s and a reference power of 6 µcal/s. Binding isotherms were plotted and analysed using Origin Software (MicroCal Inc.).

Caspase activity assay (DEVDase)

2 x 10^5 cells (MEFs) were plated in 6-well plates and treated as indicated in 2 ml for the indicated times. After treatment, media was removed, and 300 µl 1 % DISC lysis buffer (20 mM Tris-HCL pH 7.5, 150 mM NaCl, 2 mM EDTA, 1 % Triton X-100, 10 % glycerol) was added to each well, cells were scraped and lysates were left on ice for 5 min. 50 µl of lysate per condition were transferred into a 24 well plate and 450 µl DEVDase assay mix (20 mM Ac-DEVD-AMC (Sigma), 1 mM DTT, 50 mM Tris pH 7.5, 150 mM NaCl, 0.1 % Triton X-100, and 5 % glycerol) was added to each well (NB: cell lysates were not cleared). Plates were wrapped in foil and reactions allowed to proceed by incubation at room temperature for up to 24 hrs. DEVDase activity was read at 380 nM excitation/460 nM emission.

Yeast two- and three-hybrid

The yeast strain Y2HGold (Clontech) was co-transformed with the respective bait and prey plasmids. Positive transformants were selected on minimal SD-Leu-Trp medium (Formedium). Three single colonies for each bait and prey co-transformation were patched out on fresh SD-Leu-Trp plates and grown for 2 days at 30 ºC. Each patch was resuspended in 180 µl of sterile water in a 96-well plate and replica plated onto non-selective (SD-Leu-Trp) or selective medium (SD-Leu-Trp-His), containing the indicated concentration of 3-amino-1,2,4-triazole (3-AT, Formedium). Yeast plates were incubated at 30 ºC for 1 week. UbcH5b prey vector was provided by Rachel Klevit.

Protein expression and purification

BL21 cells were transformed with pGEX6p-1-3XFLAG-TNF plasmid. One colony was picked and incubated o/n in 100 ml LB medium with 100 µg/ml ampicillin. Next day 900 ml of LB medium without AMP were added, cells were grown for 1 h at 37 °C and then 0.5 mM IPTG was added for further 4 h. Bacteria were spun for 15 min at 4000 rpm, the supernatant was discarded and the pellet was lysed in 10 ml Triton X-100 lysis buffer (10 mM Tris pH 7.5, 150 mM NaCl, 10 % glycerol and 1 % Triton X-100 with complete protease inhibitor cocktail). The lysate was sonicated and left for 15 min at 4 °C and clarified for 30 min at 140,000 rpm at 4 °C. Lysate was rotated with glutathione Sepharose beads for 4 hrs at 4 °C and 3x washed with IPPG150 buffer (0,1 % Triton X-100, 50 mM Tris pH 7.5, 150 NaCl, 5 % glycerol) were performed, followed by a final wash in PreScission cleavage buffer (50 mM Tris pH 7, 150 mM NaCl, 1 mM EDTA and 1 mM DTT). For PreScission cleavage 500 µl cleavage buffer and 30 µl PreScission enzyme were added to the beads at 4 °C o/n. The beads were spun, and supernatants were collected and passed through Thermo Scientific buffer exchange columns to remove bead contamination. Recombinant TNF concentration was determined on Coomassie Blue-stained polyacrylamide gel using known amount of BSA as standard, and quantitated using Image Lab software.

Proximity ligation assay (PLA)

PLA was performed according to the manufacturer's protocol using the Duolink Detection Kit (SIGMA). Cells were examined with a confocal microscope (Objective 40x, Zeiss LSM 710).

Ub Chain Composition Mass Spectrometry Analysis

Ub chains were separated on a NuPAGE 4%–12% gradient gel (Invitrogen) before in-gel digestion with trypsin and the addition of Ub-AQUA peptide internal standards according to (Kirkpatrick et al., 2006). 10 µl of each sample was directly injected onto an EASY-Spray reverse-phase column (C18, 3 µm, 100 Å, 75 µm × 15 cm) using a Dionex UltiMate 3000 high-pressure liquid chromatography system (Thermo Fisher Scientific) and analysed on a Q-Exactive mass spectrometer (Thermo Fisher Scientific) using parallel reaction monitoring (PRM), similar to (Tsuchiya et al., 2013). Data were analysed further according to (Kirkpatrick et al., 2006)

ACKNOWLEDGEMENTS

We would like to thank Afshan McCarthy, Alan Ashworth, Chris Lord, Henning Walczak, Shaomeng Wang, Lynn Wong, and Rachael Klevit for support, reagents and advice. We also thank members of the Meier lab for helpful discussions. We would like to apologize to the many authors whose work we could not cite due to space restrictions. A. A. is supported by an SNF fellowship and an MRC grant. Work in the D.K. lab is funded by Medical Research Council (U105192732), the European Research Council (309756), and the Lister Institute for Preventive Medicine. We acknowledge NHS funding to the NIHR Biomedical Research Centre.

AUTHOR CONTRIBUTIONS

A.A. designed and performed experiments of Figure 2 (2E, F and G), all the experiments of Figure 3, Figure 5 (5A, and 5C to 5F), all the experiment of Figure 6, Figure 7 (7B to 7F) and experiments in supplementary Figure S2 to S5. T.V.B. performed experiments shown in Figure 4. Sidonie Wicky-John performed experiments of Figure 1 and supplementary Figure 1. J.R. designed and performed experiments shown in Figure 2A-C. K.S. performed the experiment of Figure 7A. G.L. performed the experiment in Figure 5B. A.A. and P.M. designed and supervised the study and wrote the paper.

References

Berger, S.B., Harris, P., Nagilla, R., Kasparcova, V., Hoffman, S., Swift, B., Dare, L., Schaeffer, M., Capriotti, C., Ouellette, M., *et al.* (2015). Characterization of GSK′963: a structurally distinct, potent and selective inhibitor of RIP1 kinase. CELL DEATH DISCOVERY.

Berger, S.B., Kasparcova, V., Hoffman, S., Swift, B., Dare, L., Schaeffer, M., Capriotti, C., Cook, M., Finger, J., Hughes-Earle, A., *et al.* (2014). Cutting Edge: RIP1 Kinase Activity Is Dispensable for Normal Development but Is a Key Regulator of Inflammation in SHARPIN-Deficient Mice. Journal of immunology (Baltimore, Md. : 1950).

Bertrand, M.J., Milutinovic, S., Dickson, K.M., Ho, W.C., Boudreault, A., Durkin, J., Gillard, J.W., Jaquith, J.B., Morris, S.J., and Barker, P.A. (2008). cIAP1 and cIAP2 facilitate cancer cell survival by functioning as E3 ligases that promote RIP1 ubiquitination. Mol Cell *30*, 689-700.

Bettermann, K., Vucur, M., Haybaeck, J., Koppe, C., Janssen, J., Heymann, F., Weber, A., Weiskirchen, R., Liedtke, C., Gassler, N., *et al.* (2010). TAK1 suppresses a NEMO-dependent but NF-kappaB-independent pathway to liver cancer. Cancer Cell *17*, 481-496.

Braten, O., Livneh, I., Ziv, T., Admon, A., Kehat, I., Caspi, L.H., Gonen, H., Bercovich, B., Godzik, A., Jahandideh, S., *et al.* (2016). Numerous proteins with unique characteristics are degraded by the 26S proteasome following monoubiquitination. Proc Natl Acad Sci U S A *113*, E4639-4647.

Budhidarmo, R., and Day, C.L. (2014). The ubiquitin-associated domain of cellular inhibitor of apoptosis proteins facilitates ubiquitylation. J Biol Chem *289*, 25721-25736.

Conte, D., Holcik, M., Lefebvre, C.A., Lacasse, E., Picketts, D.J., Wright, K.E., and Korneluk, R.G. (2006). Inhibitor of apoptosis protein cIAP2 is essential for lipopolysaccharide-induced macrophage survival. Mol Cell Biol *26*, 699-708.

Conze, D.B., Albert, L., Ferrick, D.A., Goeddel, D.V., Yeh, W.C., Mak, T., and Ashwell, J.D. (2005). Posttranscriptional downregulation of c-IAP2 by the ubiquitin protein ligase c-IAP1 in vivo. Mol Cell Biol *25*, 3348-3356.

Declercq, W., Vanden Berghe, T., and Vandenabeele, P. (2009). RIP kinases at the crossroads of cell death and survival. Cell *138*, 229-232.

Dikic, I., Wakatsuki, S., and Walters, K.J. (2009). Ubiquitin-binding domains - from structures to functions. Nat Rev Mol Cell Biol *10*, 659-671.

Dondelinger, Y., Delanghe, T., Rojas-Rivera, D., Priem, D., Delvaeye, T., Bruggeman, I., Van Herreweghe, F., Vandenabeele, P., and Bertrand, M.J.M. (2017). MK2 phosphorylation of RIPK1 regulates TNF-mediated cell death. Nat Cell Biol.

Dondelinger, Y., Hulpiau, P., Saeys, Y., Bertrand, M.J., and Vandenabeele, P. (2016). An evolutionary perspective on the necroptotic pathway. Trends Cell Biol.

Dondelinger, Y., Jouan-Lanhouet, S., Divert, T., Theatre, E., Bertin, J., Gough, P.J., Giansanti, P., Heck, A.J., Dejardin, E., Vandenabeele, P., *et al.* (2015). NF-kappaB-Independent Role of IKKalpha/IKKbeta in Preventing RIPK1 Kinase-Dependent Apoptotic and Necroptotic Cell Death during TNF Signaling. Mol Cell.

Duprez, L., Takahashi, N., Van Hauwermeiren, F., Vandendriessche, B., Goossens, V., Vanden Berghe, T., Declercq, W., Libert, C., Cauwels, A., and Vandenabeele, P.

(2011). RIP kinase-dependent necrosis drives lethal systemic inflammatory response syndrome. Immunity *35*, 908-918.
Dynek, J.N., Goncharov, T., Dueber, E.C., Fedorova, A.V., Izrael-Tomasevic, A., Phu, L., Helgason, E., Fairbrother, W.J., Deshayes, K., Kirkpatrick, D.S.*, et al.* (2010). c-IAP1 and UbcH5 promote K11-linked polyubiquitination of RIP1 in TNF signalling. Embo J *29*, 4198-4209.
Ea, C.K., Deng, L., Xia, Z.P., Pineda, G., and Chen, Z.J. (2006). Activation of IKK by TNFalpha requires site-specific ubiquitination of RIP1 and polyubiquitin binding by NEMO. Mol Cell *22*, 245-257.
Elliott, P.R., Leske, D., Hrdinka, M., Bagola, K., Fiil, B.K., McLaughlin, S.H., Wagstaff, J., Volkmar, N., Christianson, J.C., Kessler, B.M.*, et al.* (2016). SPATA2 Links CYLD to LUBAC, Activates CYLD, and Controls LUBAC Signaling. Mol Cell *63*, 990-1005.
Etemadi, N., Chopin, M., Anderton, H., Tanzer, M.C., Rickard, J.A., Abeysekera, W., Hall, C., Spall, S.K., Wang, B., Xiong, Y.*, et al.* (2015). TRAF2 regulates TNF and NF-kappaB signalling to suppress apoptosis and skin inflammation independently of Sphingosine kinase 1. eLife *4*.
Haas, T.L., Emmerich, C.H., Gerlach, B., Schmukle, A.C., Cordier, S.M., Rieser, E., Feltham, R., Vince, J., Warnken, U., Wenger, T.*, et al.* (2009). Recruitment of the linear ubiquitin chain assembly complex stabilizes the TNF-R1 signaling complex and is required for TNF-mediated gene induction. Mol Cell *36*, 831-844.
Hicke, L., Schubert, H.L., and Hill, C.P. (2005). Ubiquitin-binding domains. Nat Rev Mol Cell Biol *6*, 610-621.
Hjerpe, R., Aillet, F., Lopitz-Otsoa, F., Lang, V., England, P., and Rodriguez, M.S. (2009). Efficient protection and isolation of ubiquitylated proteins using tandem ubiquitin-binding entities. EMBO Rep *10*, 1250-1258.
Hospenthal, M.K., Mevissen, T.E., and Komander, D. (2015). Deubiquitinase-based analysis of ubiquitin chain architecture using Ubiquitin Chain Restriction (UbiCRest). Nature protocols *10*, 349-361.
Hrdinka, M., Fiil, B.K., Zucca, M., Leske, D., Bagola, K., Yabal, M., Elliott, P.R., Damgaard, R.B., Komander, D., Jost, P.J.*, et al.* (2016). CYLD Limits Lys63- and Met1-Linked Ubiquitin at Receptor Complexes to Regulate Innate Immune Signaling. Cell reports *14*, 2846-2858.
Jaco, I., Annibaldi, A., Lalaoui, N., Wilson, R., Tenev, T., Laurien, L., Kim, C., Jamal, K., Wicky John, S., Liccardi, G.*, et al.* (2017). MK2 Phosphorylates RIPK1 to Prevent TNF-Induced Cell Death. Mol Cell.
Kirkpatrick, D.S., Hathaway, N.A., Hanna, J., Elsasser, S., Rush, J., Finley, D., King, R.W., and Gygi, S.P. (2006). Quantitative analysis of in vitro ubiquitinated cyclin B1 reveals complex chain topology. Nat Cell Biol *8*, 700-710.
Kupka, S., De Miguel, D., Draber, P., Martino, L., Surinova, S., Rittinger, K., and Walczak, H. (2016). SPATA2-Mediated Binding of CYLD to HOIP Enables CYLD Recruitment to Signaling Complexes. Cell reports *16*, 2271-2280.
Lewis, J., Devin, A., Miller, A., Lin, Y., Rodriguez, Y., Neckers, L., and Liu, Z.G. (2000). Disruption of hsp90 function results in degradation of the death domain kinase, receptor-interacting protein (RIP), and blockage of tumor necrosis factor-induced nuclear factor-kappaB activation. J Biol Chem *275*, 10519-10526.
Lichti, U., Anders, J., and Yuspa, S.H. (2008). Isolation and short-term culture of primary keratinocytes, hair follicle populations and dermal cells from newborn mice and keratinocytes from adult mice for in vitro analysis and for grafting to immunodeficient mice. Nature protocols *3*, 799-810.

Mantovani, A., Allavena, P., Sica, A., and Balkwill, F. (2008). Cancer-related inflammation. Nature *454*, 436-444.
Menon, M.B., Gropengiesser, J., Fischer, J., Novikova, L., Deuretzbacher, A., Lafera, J., Schimmeck, H., Czymmeck, N., Ronkina, N., Kotlyarov, A.*, et al.* (2017). p38MAPK/MK2-dependent phosphorylation controls cytotoxic RIPK1 signalling in inflammation and infection. Nat Cell Biol.
Micheau, O., and Tschopp, J. (2003). Induction of TNF receptor I-mediated apoptosis via two sequential signaling complexes. Cell *114*, 181-190.
Moquin, D.M., McQuade, T., and Chan, F.K. (2013). CYLD deubiquitinates RIP1 in the TNFalpha-induced necrosome to facilitate kinase activation and programmed necrosis. PLoS One *8*, e76841.
Moulin, M., Anderton, H., Voss, A.K., Thomas, T., Wong, W.W., Bankovacki, A., Feltham, R., Chau, D., Cook, W.D., Silke, J.*, et al.* (2012). IAPs limit activation of RIP kinases by TNF receptor 1 during development. Embo J *31*, 1679-1691.
O'Donnell, M.A., Legarda-Addison, D., Skountzos, P., Yeh, W.C., and Ting, A.T. (2007). Ubiquitination of RIP1 regulates an NF-kappaB-independent cell-death switch in TNF signaling. Curr Biol *17*, 418-424.
Pasparakis, M., and Vandenabeele, P. (2015). Necroptosis and its role in inflammation. Nature *517*, 311-320.
Peltzer, N., Darding, M., and Walczak, H. (2016). Holding RIPK1 on the Ubiquitin Leash in TNFR1 Signaling. Trends Cell Biol.
Quistad, S.D., and Traylor-Knowles, N. (2016). Precambrian origins of the TNFR superfamily. Cell Death Discov *2*, 16058.
Samuel, T., Welsh, K., Lober, T., Togo, S.H., Zapata, J.M., and Reed, J.C. (2006). Distinct BIR domains of cIAP1 mediate binding to and ubiquitination of tumor necrosis factor receptor-associated factor 2 and second mitochondrial activator of caspases. J Biol Chem *281*, 1080-1090.
Schlicher, L., Wissler, M., Preiss, F., Brauns-Schubert, P., Jakob, C., Dumit, V., Borner, C., Dengjel, J., and Maurer, U. (2016). SPATA2 promotes CYLD activity and regulates TNF-induced NF-kappaB signaling and cell death. EMBO Rep *17*, 1485-1497.
Silke, J. (2011). The regulation of TNF signalling: what a tangled web we weave. Curr Opin Immunol *23*, 620-626.
Ting, A.T., and Bertrand, M.J. (2016). More to Life than NF-kappaB in TNFR1 Signaling. Trends Immunol *37*, 535-545.
Tracey, K.J., Beutler, B., Lowry, S.F., Merryweather, J., Wolpe, S., Milsark, I.W., Hariri, R.J., Fahey, T.J., 3rd, Zentella, A., Albert, J.D.*, et al.* (1986). Shock and tissue injury induced by recombinant human cachectin. Science *234*, 470-474.
Tsuchiya, H., Tanaka, K., and Saeki, Y. (2013). The parallel reaction monitoring method contributes to a highly sensitive polyubiquitin chain quantification. Biochem Biophys Res Commun *436*, 223-229.
Vandenabeele, P., and Bertrand, M.J. (2012). The role of the IAP E3 ubiquitin ligases in regulating pattern-recognition receptor signalling. Nat Rev Immunol *12*, 833-844.
Vanlangenakker, N., Vanden Berghe, T., Bogaert, P., Laukens, B., Zobel, K., Deshayes, K., Vucic, D., Fulda, S., Vandenabeele, P., and Bertrand, M.J. (2011). cIAP1 and TAK1 protect cells from TNF-induced necrosis by preventing RIP1/RIP3-dependent reactive oxygen species production. Cell Death Differ *18*, 656-665.

Vince, J.E., Chau, D., Callus, B., Wong, W.W., Hawkins, C.J., Schneider, P., McKinlay, M., Benetatos, C.A., Condon, S.M., Chunduru, S.K.*, et al.* (2008). TWEAK-FN14 signaling induces lysosomal degradation of a cIAP1-TRAF2 complex to sensitize tumor cells to TNFalpha. J Cell Biol *182*, 171-184.

Vince, J.E., Pantaki, D., Feltham, R., Mace, P.D., Cordier, S.M., Schmukle, A.C., Davidson, A.J., Callus, B.A., Wong, W.W., Gentle, I.E.*, et al.* (2009). TRAF2 must bind to cellular inhibitors of apoptosis for tumor necrosis factor (tnf) to efficiently activate nf-{kappa}b and to prevent tnf-induced apoptosis. J Biol Chem *284*, 35906-35915.

Wagner, S.A., Satpathy, S., Beli, P., and Choudhary, C. (2016). SPATA2 links CYLD to the TNF-alpha receptor signaling complex and modulates the receptor signaling outcomes. EMBO J *35*, 1868-1884.

Walczak, H. (2011). TNF and ubiquitin at the crossroads of gene activation, cell death, inflammation, and cancer. Immunol Rev *244*, 9-28.

Walczak, H. (2013). Death receptor-ligand systems in cancer, cell death, and inflammation. Cold Spring Harbor perspectives in biology *5*, a008698.

Wang, L., Du, F., and Wang, X. (2008). TNF-alpha induces two distinct caspase-8 activation pathways. Cell *133*, 693-703.

Yagi, H., Ishimoto, K., Hiromoto, T., Fujita, H., Mizushima, T., Uekusa, Y., Yagi-Utsumi, M., Kurimoto, E., Noda, M., Uchiyama, S.*, et al.* (2012). A non-canonical UBA-UBL interaction forms the linear-ubiquitin-chain assembly complex. EMBO Rep *13*, 462-468.

Yatim, N., Jusforgues-Saklani, H., Orozco, S., Schulz, O., Barreira da Silva, R., Reis e Sousa, C., Green, D.R., Oberst, A., and Albert, M.L. (2015). RIPK1 and NF-kappaB signaling in dying cells determines cross-priming of CD8(+) T cells. Science *350*, 328-334.

Zheng, C., Kabaleeswaran, V., Wang, Y., Cheng, G., and Wu, H. (2010). Crystal structures of the TRAF2: cIAP2 and the TRAF1: TRAF2: cIAP2 complexes: affinity, specificity, and regulation. Mol Cell *38*, 101-113.

FIGURE LEGENDS

Figure 1. The UBA domain of cIAP1 interacts with TRAF2

(A) Schematic representation of the domain architecture of cIAPs and TRAF2, and the interaction between cIAPs and TRAF2. **(B)** Schematic representation of the putative interaction partners of cIAP1, identified by yeast two-hybrid using the C-terminal portion (encompassing the UBA/CARD/RING region) of cIAP1 as bait. **(C-F)** Yeast two-hybrid analysis studying the interaction between the indicated cIAP1 fragments and TRAF2 variants. Shown are three single colonies for each cotransformation grown on nonselective (SD-Leu-Trp) or selective medium (SD-Leu-Trp-His, containing the indicated 3AT concentration).

Figure 2. cIAP2 requires a functional UBA domain to efficiently interact with TRAF2

(A-C) Binding of the indicated cIAP2 fragments to TRAF2 was measured by Isothermal Titration Calorimetry. K_D: Binding constant. Note, the data shown in (A) was previously published (Zheng et al., 2010) and is shown for comparison reason. **(D)** Schematic diagram of the *Flp-In*^{TM}*T-REx*^{TM}*-HEK293*^{shcIAP1} cell system in which endogenous *cIAP1* was knocked down via inducible expression of *mir30*-based short hairpin RNA targeting *cIAP1*'s 30 UTR. These cells also carry a single *FRT* site that allows Flp-mediated integration of transgenes into the same transcriptionally regulatable genomic locus. Expression of the transgene and the *mir30*-based *shcIAP1* are induced following treatment with Doxocycline (Dox). *TRE*, tetracyclin response element; UBC, ubiquitin promoter; FRT, flippase recognition target; Tet Op, tetracycline operon; Tet-R, tet repressor protein; rtTA3, reverse Tet transactivator (rtTA3). **(E)** Western blot analysis of *Flp-In* cells treated for 72 hrs with Dox (100 ng/ml), to allow expression of the indicated transgenes, followed by treatment with the SMAC mimetic (SM) Compound A (100 nM) for 6 hrs. **(F and G)** Biotinylated SM was used to purify IAPs from lysates of *Flp-In* cells that were treated with Dox for 72 hrs. TRAF2-binding was then assessed by immunoblotting. In parallel, expression levels of cIAP1 and TRAF2 were controlled by immunoblotting total cell lysates with the respective antibodies. Representative immunoblots are shown of at least three independent experiments.

Figure 3. Mice with a knock-in mutation in the UBA domain develop normally and do not exhibit defects in the canonical and non-canonical NF-κB activation

(A) Gene targeting strategy for the generation of mice with conditional deletion of cIAP2 and conditional mutation of the UBA domain of cIAP1. Exon 2 and 3 of *cIAP2* were flanked by FRT sites. To generate the UBA mutation, M396 and F398 were mutated to A396 and A398, respectively. A targeting vector containing a lox-P flanked-minigene spanning exon 4 to 7 of cIAP1 followed by a stop sequence and a hygromycin resistance sequence was used to ensure the WT expression of cIAP1 and therefore the conditional expression of the UBA mutation. **(B)** Expected and observed numbers of mice with the respective genotypes. **(C)** Western blot analysis of cIAP1 protein levels of *WT* and *cIAP1*^{UBAmut} MEFs obtained from three different embryos. **(D)** Biotinylated SM was used to purify IAPs from lysates of *cIAP2*$^{-/-}$

and *cIAP1*^{UBAmut} MEFs. TRAF2-binding was then assessed by immunoblotting. In parallel, expression levels of cIAP1 and TRAF2 were controlled by immunoblotting total cell lysates with the respective antibodies. **(E)** Purification of the TNF-receptor signalling complex (complex-I) from immortalized MEFs. Cells of the indicated genotypes were treated with FLAG-TNF for 0, 5 and 60 mins. Cell lysates were then subjected to FLAG immune-precipitation followed by Western blot analysis with the indicated antibodies. Representative images of at least three independent experiments are shown. **(F)** Western blot analysis of *cIAP2*$^{-/-}$ and *cIAP1*^{UBAmut} MEFs treated with SM (100 nM) and TWEAK for 6 hrs, followed by Western blot analysis using the indicated antibodies. **(G)** Western blot analysis of MEFs with the indicated genotypes treated with TNF and harvested at the indicated times points. **(H and I)** The presence of relative mRNA levels (H) and cytokines in the culture media (I) of MEFs treated with TNF (10 ng/ml) for the indicated time points were analysed by RT-PCR and ELISA, respectively. **(J and K)** Primary *WT* and *cIAP1*^{UBAmut} BMDMs and keratinocytes were treated with TNF (10 ng/ml) for 2 and 6 hrs, and mRNA levels of the indicated cytokines were measured by RT-PCR.

Figure 4. Mice with a knock-in mutation in the UBA domain develop normally but are acutely sensitive to TNF-induced systemic inflammatory response syndrome (SIRS)

(A and B) Body temperature and survival of *WT* (D, n=11; E, n=12) and corresponding littermate *cIAP1*^{UBAmut} (D, n=8) or *cIAP2*$^{-/-}$ (E, n=11) mice injected with 4 µg of mTNF. Data are representative of two independent experiments. Survival curves were compared using log-rank Mantel-Cox test (* $p<0.05$, *** $p<0.001$). **(C and D)** Plasma samples of *WT* and *cIAP1*^{UBAmut} (F) or *cIAP2*$^{-/-}$ (G) mice were collected at the indicated time points following challenge with mTNF (4 µg, i.v.) and analysed for activities of LDH, AST and ALT. n=4 per time point and genotype. Data are presented as mean ± SD, ** $p<0.01$, statistics were performed using two-way ANOVA. **(E and F)** TUNEL staining and quantification of liver sections of *WT* and *cIAP1*^{UBAmut} mice used in C and D. Of note, data shown in A and B were obtained from two sets of animals, while the data shown in C-F were obtained from a third set of animals.

Figure 5. Mutation in the UBA domain switches the TNF response to cell death

(A, C, E) Primary BMDMs (A), MDFs (C) and MEFs (E) of the indicated genotypes were treated as shown (TNF 100 ng/ml, GSK'963 100 nM, SM 100 nM, for BMDMs TNF 1 ng/ml) for 24 hrs followed by quantification of Propidium Iodide (PI) positive cells. Data are presented as mean ± SD, n>3, * $p<0.05$ *** $p<0.001$, statistics were performed using two-way ANOVA. **(B)** PLA of primary BMDMs from *cIAP2*$^{-/-}$ and *cIAP1*^{UBAmut} animals using RIPK1 and RIPK3 antibodies. Cells were stimulated with 1 ng/ml TNF for the indicated time points. The graph to the side indicates the quantification of RIPK1/RIPK3 PLA speckles. **(D and F)** Primary MDFs (D) and MEFs (F) of the indicated genotypes were treated for 4 hrs as indicated (TNF 100 ng/ml, z-VAD-FMK 10 µM), followed by FADD immuno-precipitation and

Western blot analysis for the indicated proteins. Images are representative of at least three independent experiments.

Figure 6. The UBA directly regulates RIPK1 ubiquitylation

(A and B) Purification of the TNF-R1 signalling complex (complex-I) from primary MEFs (A) and MDFs (B). Cells of the indicated genotypes were treated with FLAG-TNF for 0, 5 and 60 mins. Cell lysates were then subjected to FLAG immune-precipitation followed by Western blot analysis with the indicated antibodies. Representative images of at least three independent experiments are shown. **(C)** Purification of the TNF-R1 signalling complex (complex-I) from immortalized *cIAP2*$^{-/-}$ and *cIAP1*^{UBAmut} MEFs reconstituted either with empty vector (control) or a doxycycline inducible construct encoding *cIAP1*^{UBAmut}.

Figure 7. UBA-mediated ubiquitylation of RIPK1 represses its kinase activity and facilitates RIPK1 degradation in response to TNF

(A) Absolute quantification (AQUA)-based mass spectrometry of RIPK1 in complex-I. The scheme indicates the double purification strategy to isolate RIPK1 in complex-I. Pie charts indicating the ubiquitin linkage types detected on RIPK1 in complex-I from *cIAP2*$^{-/-}$ and *cIAP1*^{UBAmut} MEFs in two independent replicates. **(B)** UbiCRest analysis of ubiquitylated RIPK1 in complex-I. Complex-I was purified from *cIAP2*$^{-/-}$ and *cIAP1*^{UBAmut} MEFs using FLAG-TNF as affinity reagent. Immuno-complexes were then subjected to UbiCRest analysis using the indicated DUBs followed by Western blot analysis for RIPK1. **(C)** *cIAP2*$^{-/-}$ and *cIAP1*^{UBAmut} MEFs were treated with TNF (100 ng/ml) for the indicated time points. Lysates were then split in two and subjected either to FADD immune-precipitation (complex-II) or TUBE pull-down (ubiquitylated proteome), followed by Western blot analysis with the indicated antibodies. Representative images of at least three independent experiments are shown. **(D)** *cIAP1*^{UBAmut} MEFs were incubated for 1 hr with MG132 (20 μM) or left untreated and then subjected to TNF stimulation for the indicated time points. TUBE pull-down was then carried out on cell lysates followed by Western blot analysis with the indicated antibodies. **(E)** Immunoprecipitation of RIPK1 in *cIAP2*$^{-/-}$ and *cIAP1*^{UBAmut} MEFs followed by immunoblotting analysis with the indicated antibodies. **(F)** *cIAP2*$^{-/-}$ and *cIAP1*^{UBAmut} MDFs were treated as indicated for 24 hrs (TNF 100 ng/ml, TPCA-1 1 μM) followed by quantification of Propidium Iodide (PI) positive cells.

Supplementary Information

Supplementary Figure S1. Interaction of the UBA domain of cIAP1 with TRAF2, Related to Figure 1

(A-C) Yeast two-hybrid negative control. The indicated bait constructs were co-transformed with the empty prey vector pACT2 to rule out autonomous growth.

Supplementary Figure S2. The UBA domain of cIAP1 is dispensable for normal development and NF-KB-induced gene expression, Related to Figure 3

(A) Aging curves for *WT* and *cIAP1*^{UBAmut} mice. **(B)** Representative images of 2 months old *WT* and *cIAP1*^{UBAmut} mice. **(C)** FACS analysis of hematopoietic cells isolated from the spleen of *WT* and *cIAP1*^{UBAmut} mice. Cells were analysed using antibodies for the indicated cell surface markers. **(D)** RT-PCR analysis of *cIAP2* mRNA levels in *WT*, *cIAP2*$^{-/-}$ and *cIAP1*^{UBAmut} MEFs. **(E)** TUBE affinity purification of the ubiquitylated proteome from *WT* and *cIAP1*^{UBAmut} MEFs treated with the indicated agents. TUBE pull-down was followed by Western blot analysis with the indicated antibodies. **(F)** Western blot analysis of MDFs with the indicated genotypes treated with TNF and harvested at the indicated times points.

Supplementary Figure S3. Mutation in the UBA domain switches the TNF response to cell death, Related to Figure 5

(A-C) Primary MEFs of the indicated genotypes were treated with TNF (100 ng/ml) for 24 hrs followed by quantification of PI positive cells. **(D)** *WT* and *cIAP1*^{UBAmut} primary MEFs were transfected either with siRNA control or with siRNAs targeting *Mlkl*. After 72 hrs following transfection, cells were treated as indicated, and cell death was measured by scoring PI positive cells. **(E)** DVDase analysis of primary MEFs of the indicated genotypes subjected to indicated treatments for 8 hrs (z-VAD-FMK 10 μM), data are presented as mean ± SD, n=3, * $p<0.05$, statistics were performed using two-way ANOVA. **(F)** Western blot analysis of activated caspase-8 and caspase-3 of the indicated MEFs treated with the indicated agents for 12 hrs.

Supplementary Figure S4. The UBA domain facilitates cIAP1-mediated degradation of RIPK1, Related to Figure 6

(A) Purification of the TNF-receptor signalling complex (complex-I) from primary MEFs of the indicated genotypes. Cells of the indicated genotypes were treated with FLAG-TNF for 0, 5 and 60 mins. Cell lysates were then subjected to FLAG immune-precipitation followed by Western blot analysis with the indicated antibodies. Representative images of at least three independent experiments are shown.

Supplementary Figure S5. cIAP1 targets RIPK1 to proteasomal degradation, Related to Figure 7

(A) *WT* MEFs, either pre-incubated with MG132 for 1 hour or left untreated, were treated with TNF (100 ng/Ml) for the indicated time points. Cell lysates were subjected to TUBE pull-down followed by USP2 digestion. Western blot analysis for the indicated proteins was then carried out. **(B)** WT MEFs were treated with the pan-DUB inhibitor PR619 for 2 hrs. Cell lysates were subjected to TUBE pulldown followed by Western blot analysis using an Ubiquitin specific antibody. **(C)** WT MEFs were treated with TNF in the presence of the pan-DUB inhibitor PR619 for 2 hrs, and complex-I was purified using FLAG-TNF as affinity reagent. The presence of the indicated proteins was analysed using the indicated antibodies.

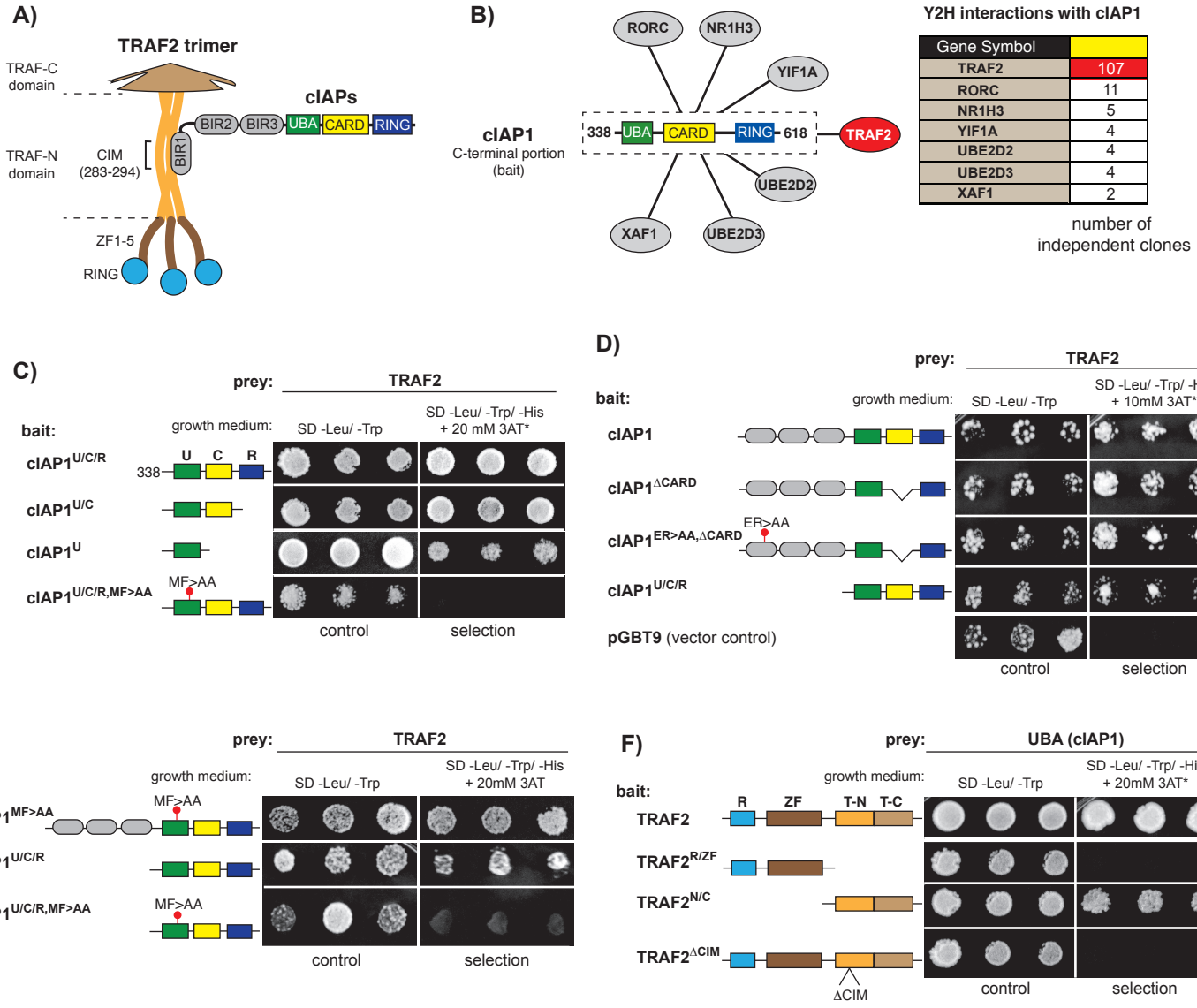

Figure 1
Annibaldi et al., 2017

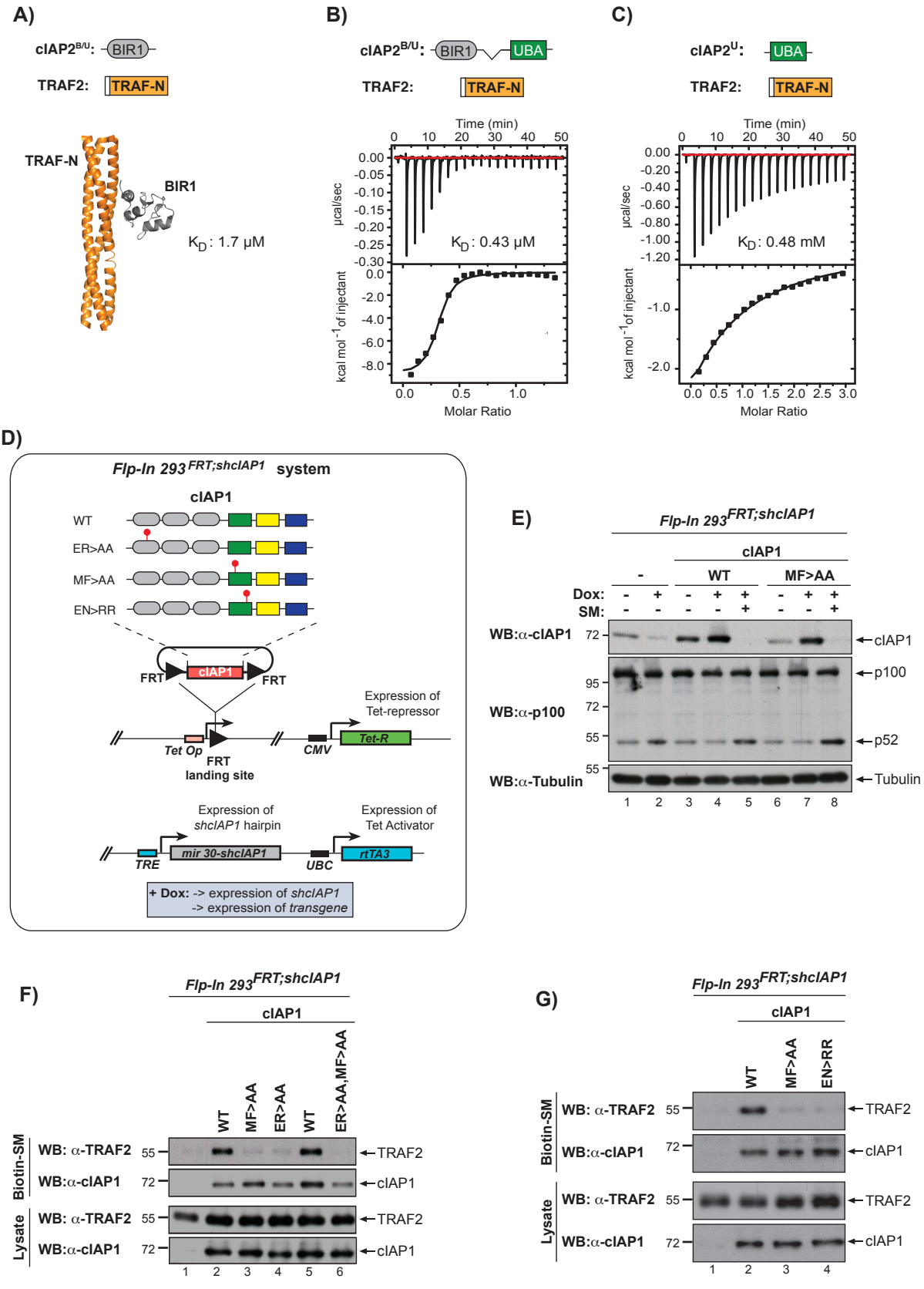

Figure 2
Annibaldi et al., 2017

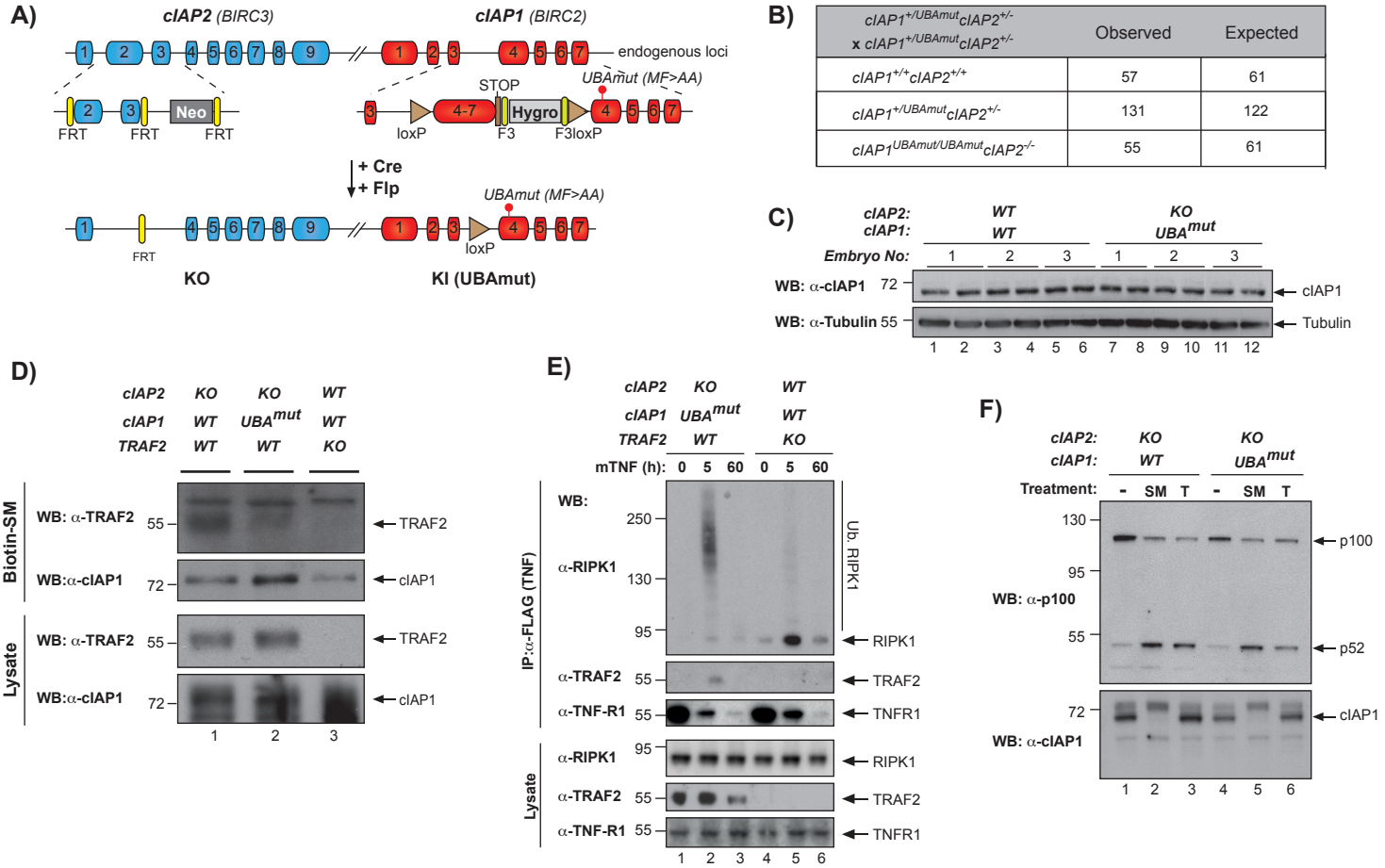

$cIAP1^{+/UBAmut}cIAP2^{+/-}$ x $cIAP1^{+/UBAmut}cIAP2^{+/-}$	Observed	Expected
$cIAP1^{+/+}cIAP2^{+/+}$	57	61
$cIAP1^{+/UBAmut}cIAP2^{+/-}$	131	122
$cIAP1^{UBAmut/UBAmut}cIAP2^{-/-}$	55	61

Figure 3
Annibaldi et al., 2017

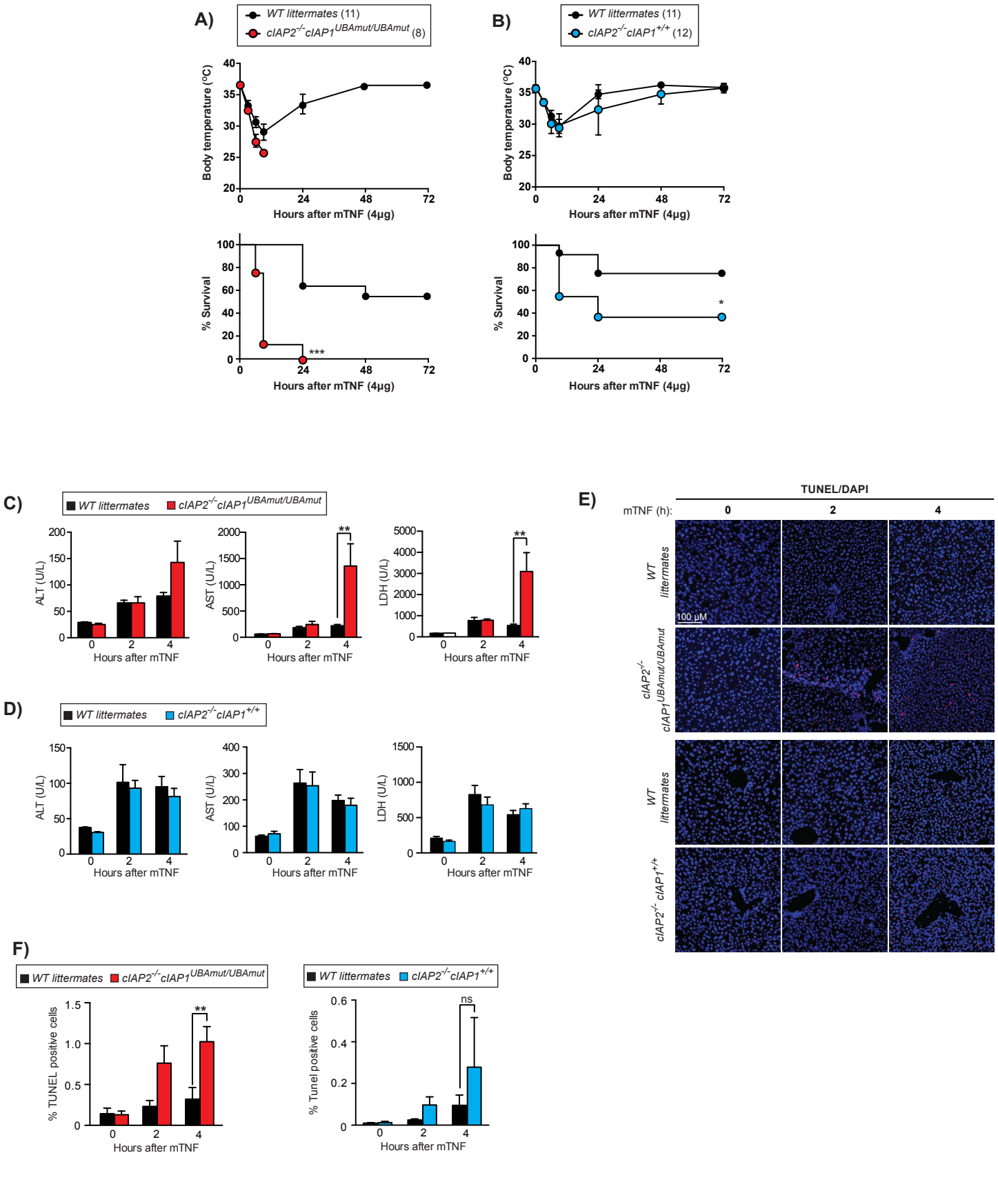

Figure 4
Annibaldi et al., 2017

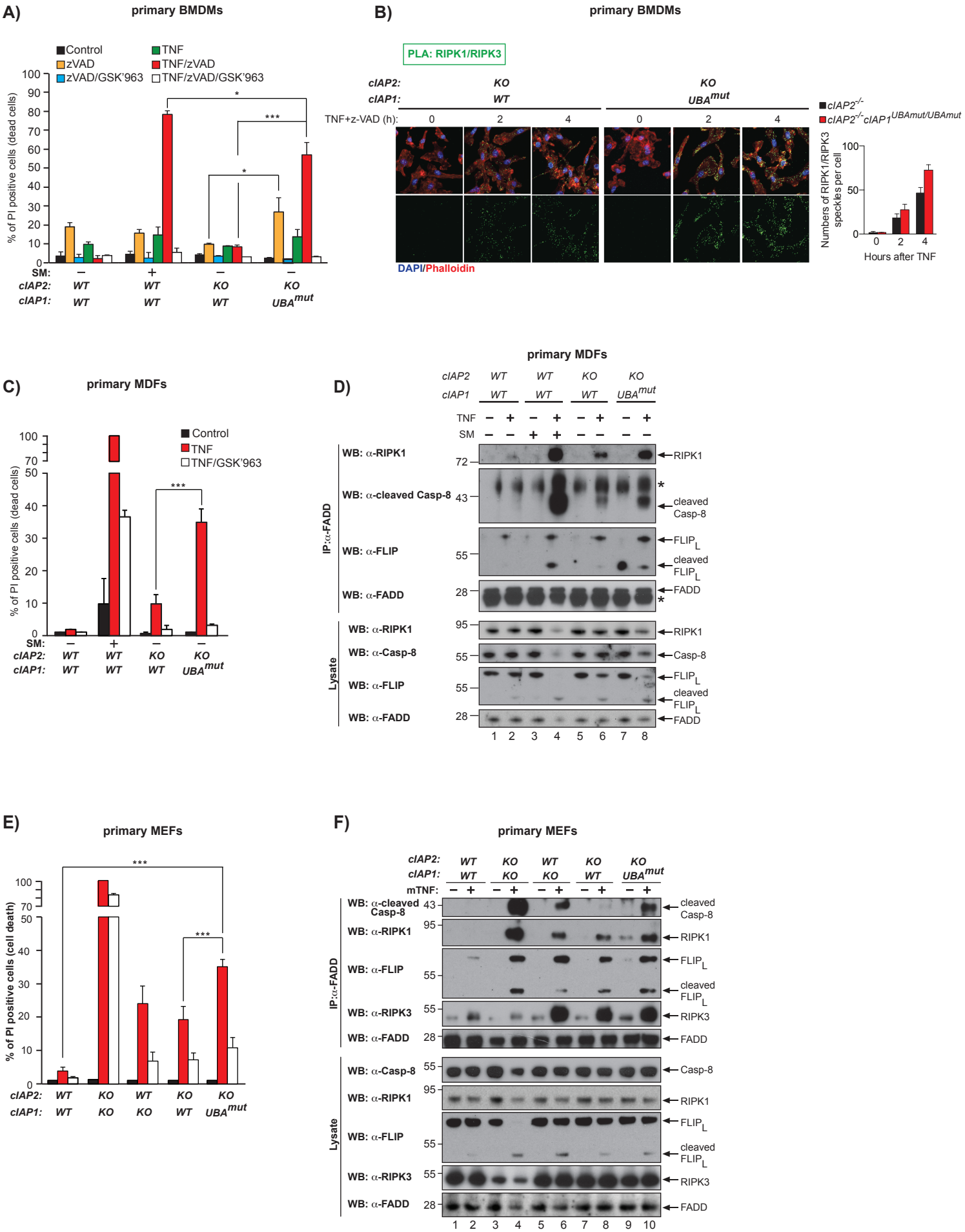

Figure 5
Annibaldi et al., 2017

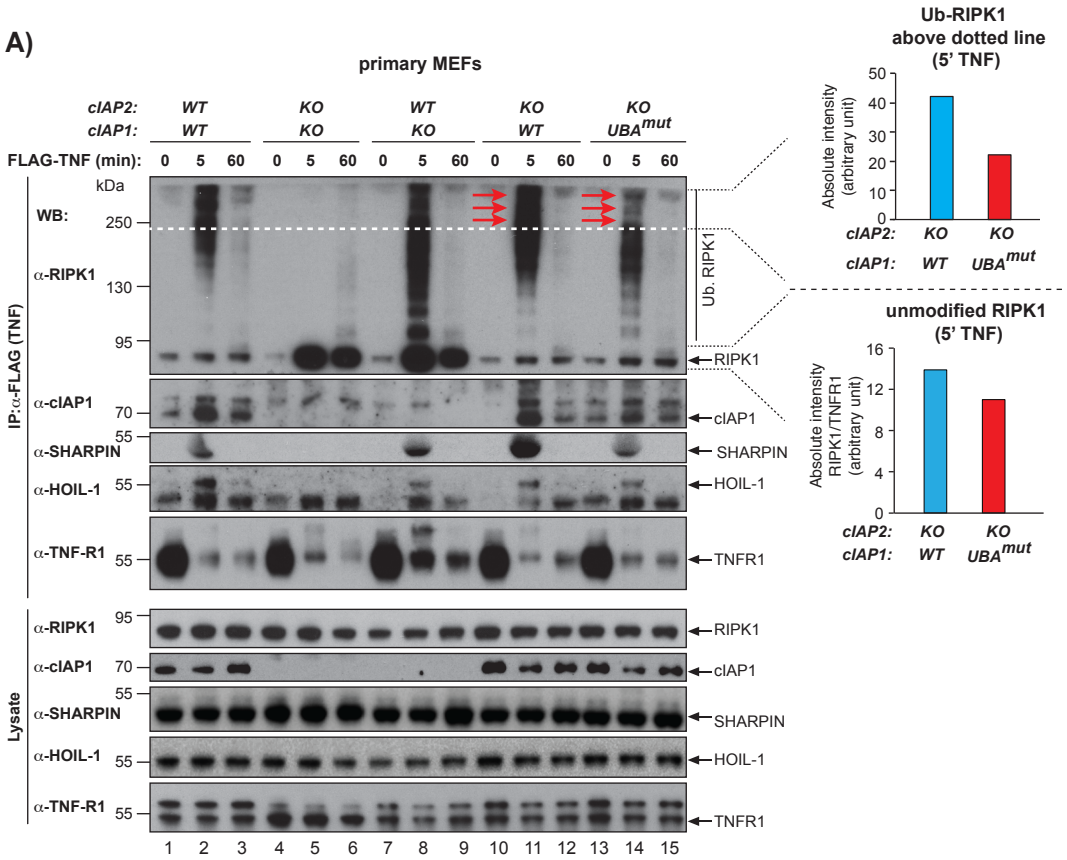

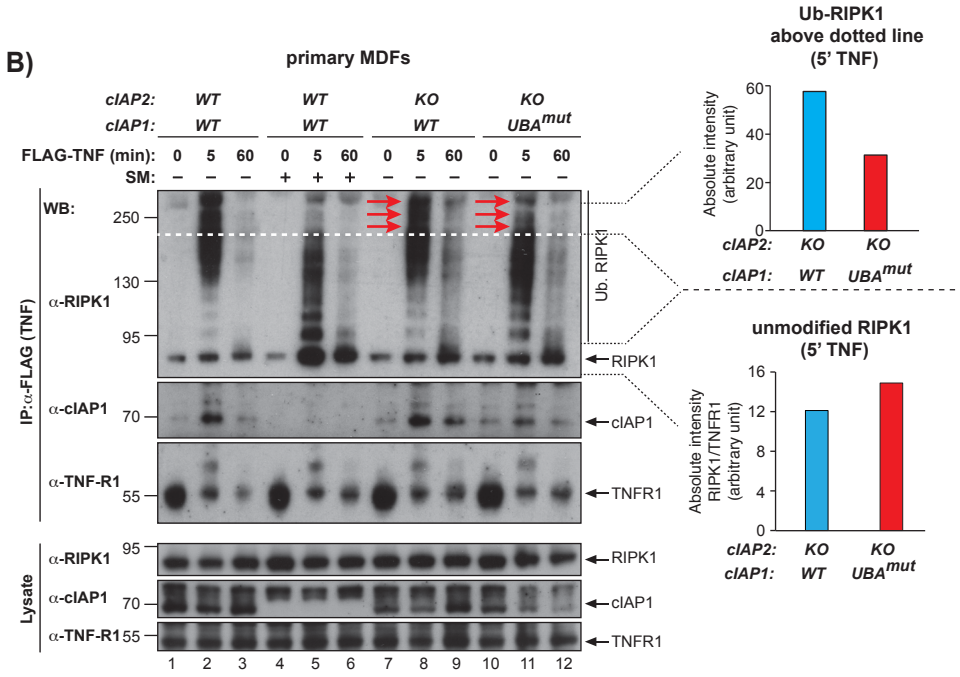

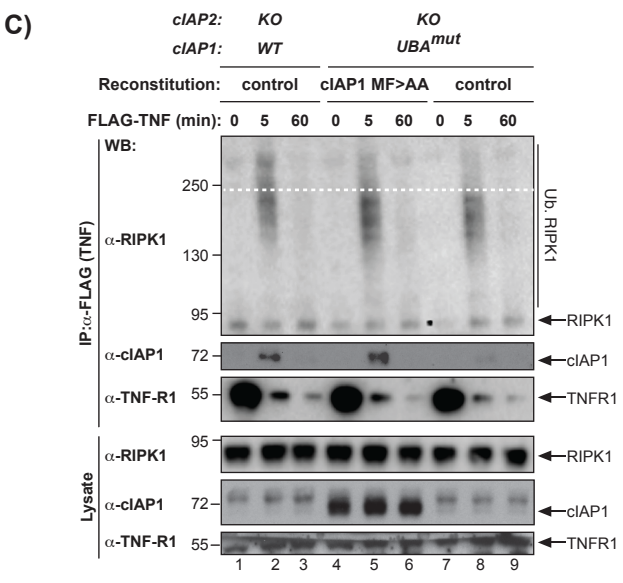

Figure 6
Annibaldi et al., 2017

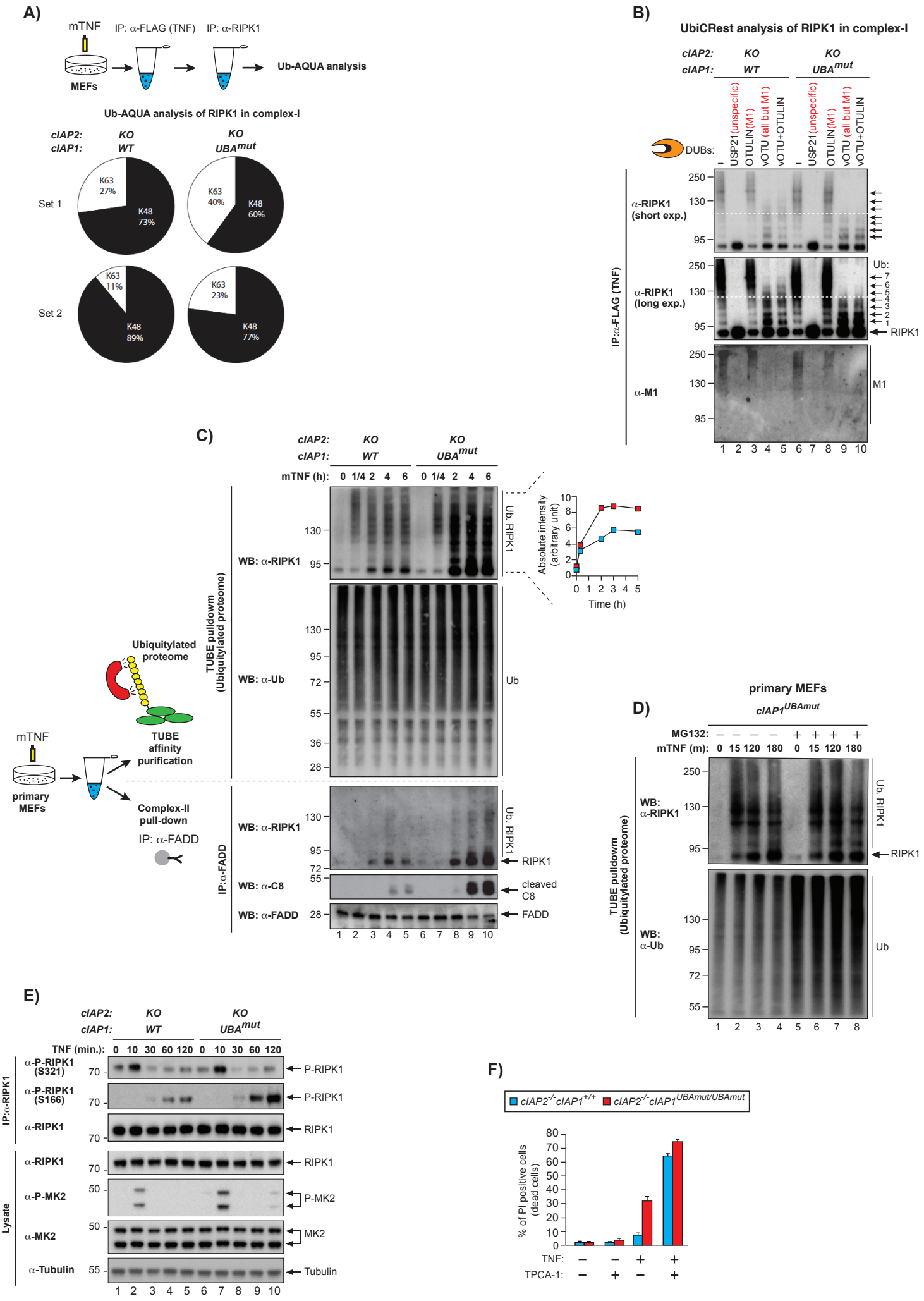

Figure 7
Annibaldi et al., 2017

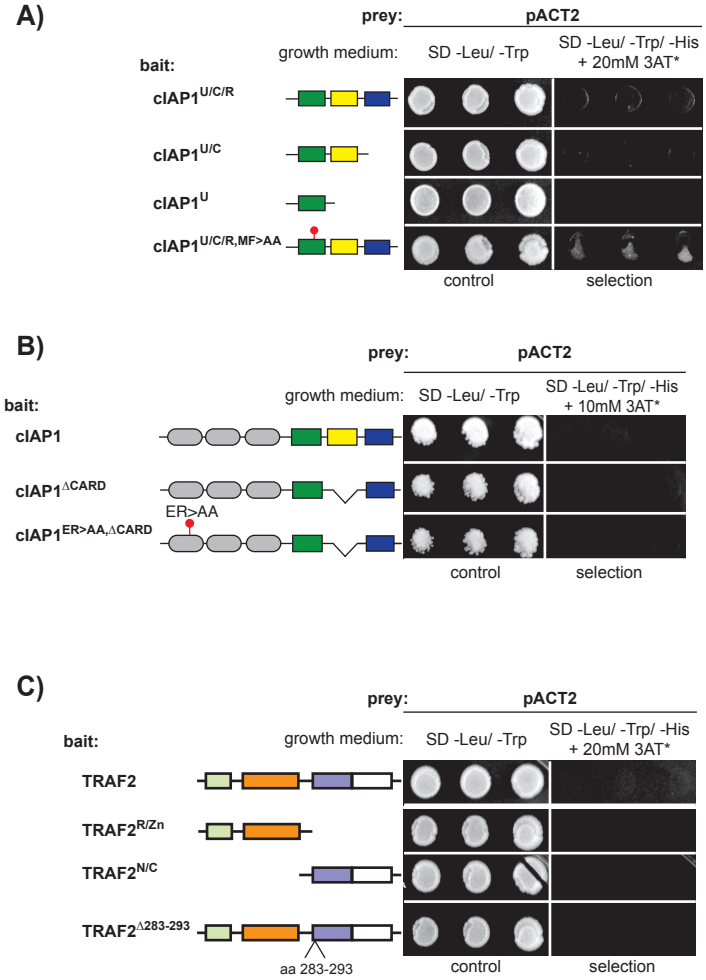

Suppl. Figure S1
Annibaldi et al., 2017

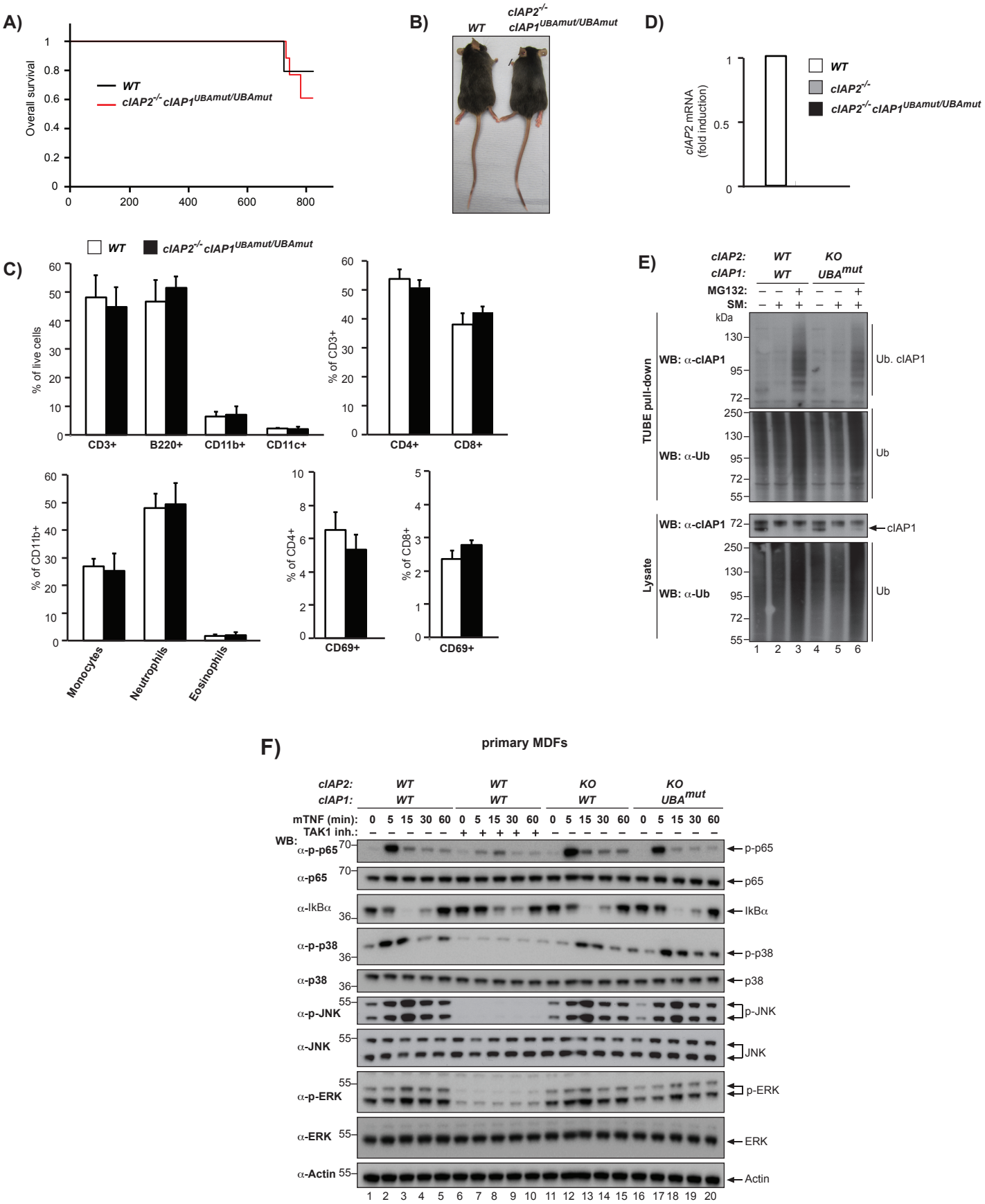

Suppl. Figure S2
Annibaldi et al., 2017

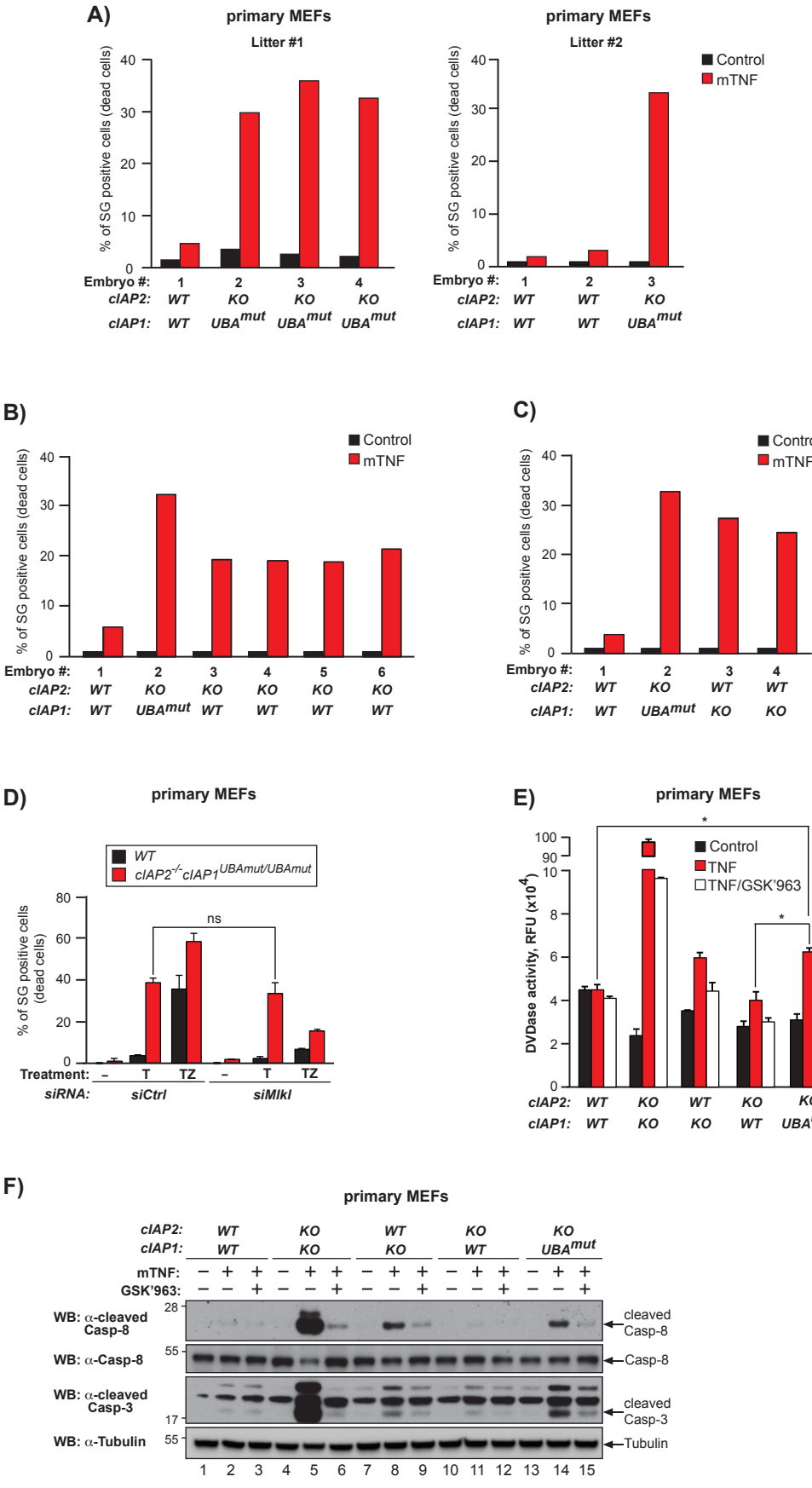

Suppl. Figure S3
Annibaldi et al., 2017

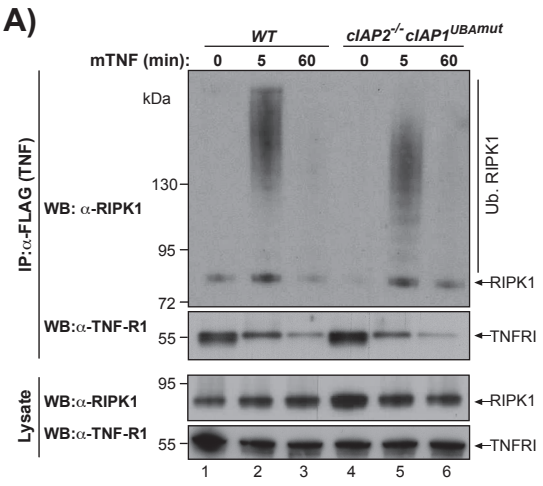

Suppl. Figure S4
Annibaldi et al., 2017

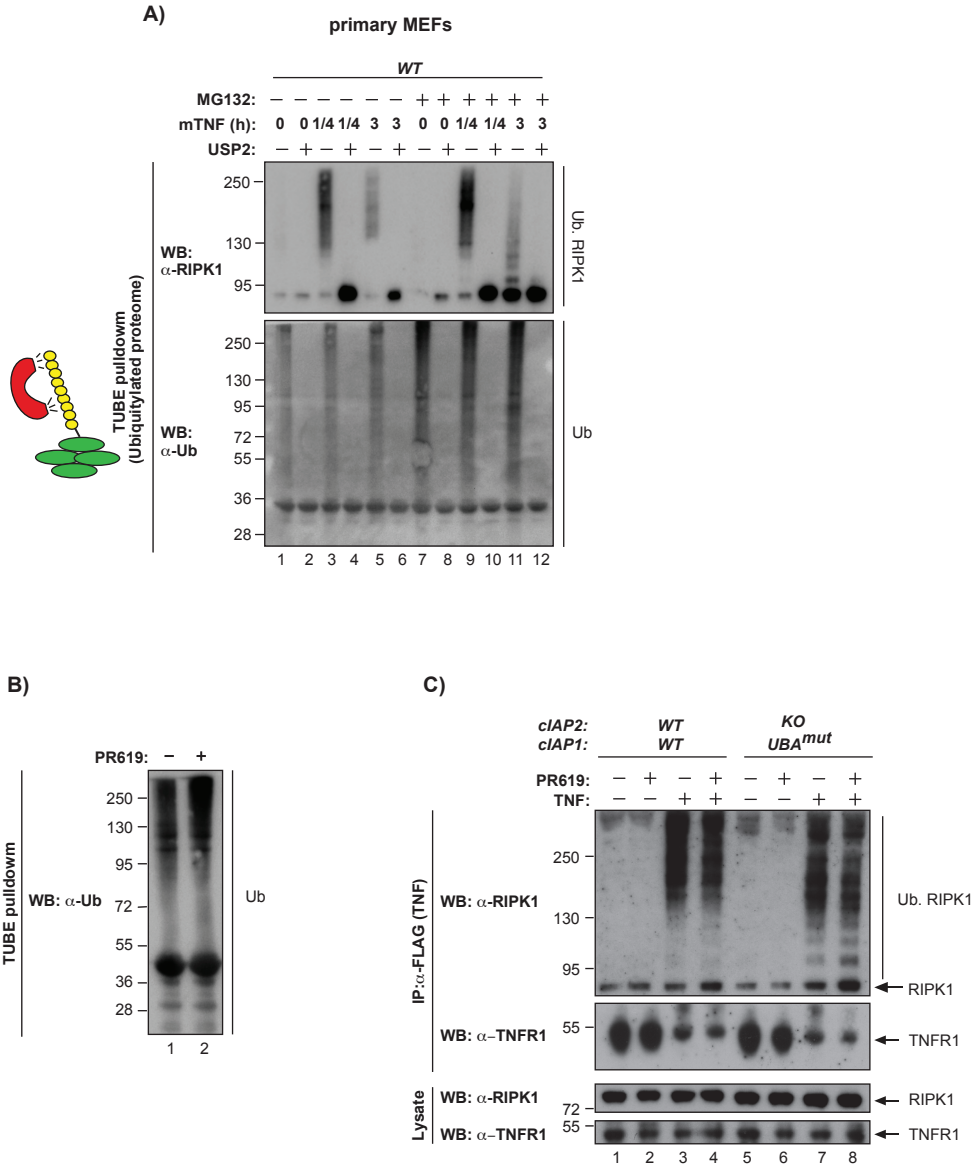

Suppl. Figure S5
Annibaldi et al., 2017